Journal of Neuroinflammation

RESEARCH

Open Access

A systematic scoring system to optimise the testing of neurotherapeutics in models of perinatal brain injury, with an applied case study of human umbilical-cord MSC

Cindy Bokobza[1,4*†], Clémence Réda[1†], Syam Nair[2,3†], David Guenoun[1,4], Eridan Rocha-Ferreira[2,3], Valérie Faivre[1], Tifenn Le Charpentier[1], Cora Nijboer[5], Caroline de Theije[5], Sophie Lebon[1], Joakim Ek[2,3], Mohamed Gaeth Hafez[2,3], Leslie Schwendimann[1], Médine Benchouaia[6], Sophie Lemoine[6], Giorgia Volpi[7], Katiuscia Dallaglio[7], Nicola Pelizzi[8], Bobbi Fleiss[1,9*], Juliette Van Steenwinckel[1], Andrée Delahaye-Duriez[1,10,11†], Henrik Hagberg[2,3†], Pierre Gressens[1†] and on behalf of the PREMSTEM consortium

Abstract

The preclinical stages of therapeutic agent development cost hundreds of millions of dollars, stymying innovation and slowing the development of products to improve human health. There is a striking unmet need for therapies that protect or repair the brain damage associated with preterm birth, i.e., delivery before 37 weeks of gestation. Of the more than 15 million babies born preterm every year, up to 60% will go on to develop a neurological disorder, with the earliest-born infants the most impacted. We have limited options with limited efficacy for preventing or treating these changes. Combining accurate knowledge of pathophysiology with high-throughput sequencing and computational biology approaches is a logical step towards an optimised screening pipeline. In this study, we conducted comprehensive testing of dose, timing, and route of administration, integrating multimodal data from preclinical models of brain injury common in preterm-born infants to validate the most effective therapeutic option for the cord-derived mesenchymal stem cell product (HuMSC). In this study, HuMSC serves as a working example, but the scoring system is therapy-agnostic. We developed a scoring protocol based on microglia transcriptome analyses and myelin protein expression to evaluate the efficacy of the HuMSC product in a rat model of inflammation-associated preterm infant brain injury. We identified the superiority of treatment delivered in the tertiary phase of injury over treatments in the acute or subacute stages, as well as the superiority of intranasal over intravenous delivery of HuMSCs. The optimal time, dose, and route of administration options for HuMSC were

†Cindy Bokobza, Clémence Réda and Syam Nair contributed equally to this work.

*Correspondence:
Cindy Bokobza
cindy.bokobza@inserm.fr
Bobbi Fleiss
bobbi.fleiss@rmit.edu.au

Full list of author information is available at the end of the article

confirmed in a second model relevant to preterm infants, but with a different pathophysiology, namely germinal matrix haemorrhage. In conclusion, we have established a scoring protocol that expedites the collection of comprehensive dose, time and route of administration data critical for establishing large animal and clinical trials with the greatest chance of success.

Keywords Stem cell therapy, Automated outcome scoring, Phenotype rescue, Encephalopathy of prematurity, Microglia, Neuroinflammation, Myelination, Pathway analysis

Background

Fast, accurate and cost-effective in vivo preclinical screening of novel therapeutics could significantly accelerate the drug development pipeline. Up to 40% of the approximately US$1.6 billion spent on research and development per new entity goes towards preclinical work [1]. The demand for faster, accurate in vivo validation is underscored by the growing number of high-value targets being generated by platforms that combine computational modelling and automated biophysical and in vitro screening, which still require in vivo validation [2, 3].

Perinatal brain injuries are one key area of human health in which preventative and treatment options are severely limited and only partially effective [4]. Every year, 15 million infants are born preterm, before 37 weeks of 40 weeks of gestation. One million of these infants will die, and up to 60% of those surviving preterm birth will develop brain injury. Injury to the preterm brain includes hypomyelination, reduced grey matter volumes driven by synaptic and interneuron defects, and microgliosis, collectively termed encephalopathy of prematurity (EoP). These infants are also at an increased risk of developing a germinal matrix haemorrhage (GMH), characterised by white matter damage and microgliosis. These injuries put preterm-born infants at an increased risk of developing cerebral palsy, autism spectrum disorder, attention deficit hyperactivity disorder, and seizures [5]. Preterm birth is even associated with an increased risk of adult stroke [6] and Alzheimer's disease [7]. We have no effective way to prevent or treat these injuries. As such, effective treatment of preterm-born infants presents an extraordinary opportunity for improving disability-adjusted life years (DALYs).

Advancements in clinical research have led to the validation of surrogate outcome measures that are quicker and easier to obtain than the gold standard of behaviour at two years, streamlining workflows and enhancing the efficiency of clinical trials. For example, the Centre for the Developing Brain team at King's College London substantially decreased the required patient number to test therapies to treat term infant neonatal encephalopathy [8]. This was achieved by establishing a clear correlation between two early markers of injury, early imaging for lactate to N-acetyl aspartate ratio in the thalamus and fractional anisotropy in the posterior limb of the internal capsule, and neurobehavioral outcomes at two years of age [9].

Microglia-mediated neuroinflammation and white matter injury are two early markers of injury that strongly correlate with behavioural outcomes in EoP and GMH models, and are also observed in patient cohorts [10–17]. An immune-activated state of these resident immune cells involves the production of cytokines and reactive oxygen species, which directly injure the developing brain [18, 19]. Immune activation also prevents microglia from undertaking key roles in brain development, including supporting oligodendrocyte maturation, neuronal migration, and synaptic pruning [20–22]. Exposure to maternal or foetal infection and inflammation during pregnancy is a key risk factor for the occurrence of preterm birth [23, 24], and increases the risks of EoP and long-term neurodevelopmental impairments [25–28]. Modelling EoP using exposure to a systemic inflammatory challenge [29–32] mimics the hallmarks of injury in infants with EoP, including microglial immune-reactivity, white matter injury, reduced myelin protein expression, and long-term neurocognitive impairments. GMH is a rupture of the capillary network of the subependymal germinal matrix that occurs in approximately 12% of preterm-born infants [33]. GMH modelled with intragerminal injection of collagen to disrupt tissue integrity mimics the clinical signs of GMH, including microgliosis, grey matter injury, white matter injury (reduced myelin protein expression), and long-term neurocognitive deficits [34] Andersson, 2021 #7087 [35]). As such, microglial reactivity and myelination may be key surrogates around which to build a streamlined pathway for screening therapies for perinatal brain injuries.

Mesenchymal stromal cells (MSCs) have a low immunogenicity and possess anti-inflammatory and anti-oxidative properties. They reduce microglial immune-reactivity and stimulate myelin production when applied in the context of in vitro and in vivo models of perinatal brain injury [36–40]. MSCs are safe for use in preterm-born and term-born infants, as well as in children with cerebral palsy [38, 41, 42]. However, substantial problems with the current body of evidence hinder translation and commercialisation. Studies often use poorly characterised stem cells unsuitable for commercial production. There are very few studies specifically addressing models of preterm brain injury [41, 43]. Furthermore,

comprehensive dose, timing, and route-finding studies, validated across multiple clinically relevant models, are lacking but are needed to inform clinical trial design. These comprehensive studies are costly and typically outside the reach of most laboratories. Increasing the efficacy of this type of screening was an aim of this study.

This study introduces an optimised high-throughput and multi-modal screening protocol to determine the optimal time, dose and route of administration options for treatment by a standardised human umbilical cord-derived MSCs (HuMSCs) therapy in two clinically relevant rat models of the brain injury observed in preterm-born infants – EoP [44–46] and GMH [34, 35, 47]. We evaluated administration route (intranasal, IN versus intravenous, IV), dose (20 M, 50 M and 125 M cells/kg), and delivery timing (acute, postnatal day (P)5; secondary, P10; and tertiary delivery, P20; Fig. 1). We hypothesise that microglia-enriched transcriptome profiling combined with myelin basic protein (MBP) imaging will predict HuMSC efficacy. The outcome scoring protocol we developed using a computational score based on microglial sequencing profiles and MBP revealed that intranasal treatment, delivered in the tertiary phase of injury (equivalent to 2–3 years of age in the infant), effectively reduces brain injury in our EoP and GMH models.

Methods

Animal models of brain injury relevant to preterm-born infants

Figure 1 is a schematic of modelling inflammation-associated EoP and GMH and the HuMSC treatments and analysis time points. All experimental procedures followed the ARRIVE guidelines [48] and were undertaken in line with national guidelines with prior ethical approval from Université Paris-Nord and the French Ministry of Higher Education, Research, and Innovation APAFIS #23460–2019122413519837 or the Gothenburg Animal Ethics Committee 825–2017 and 2195–19. All

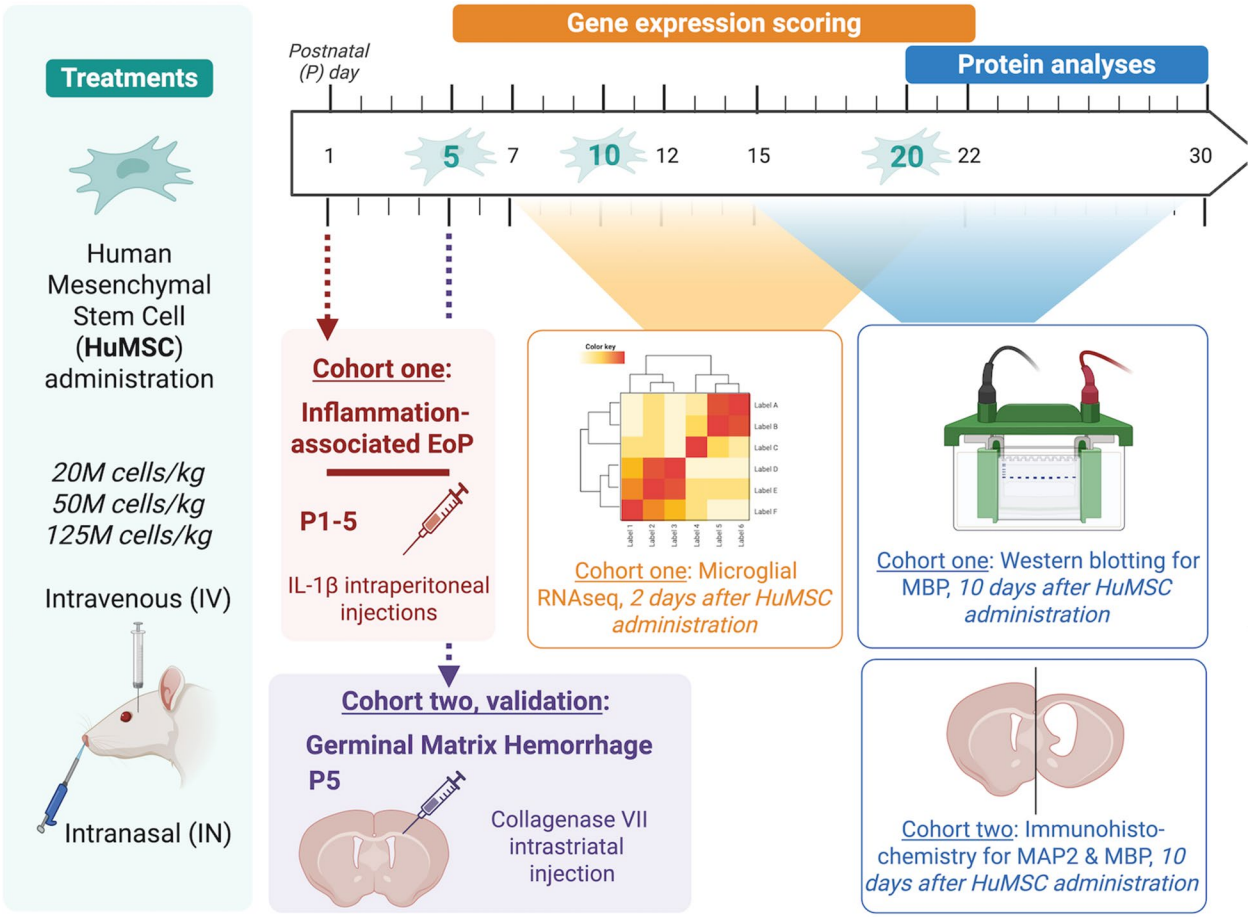

Fig. 1 An outline of our optimised high through-put in vivo screening protocol for determining the ideal treatment paradigm for human umbilical cord-derived MSCs (HuMSCs) in two rat models of perinatal brain injury: inflammation-induced encephalopathy of prematurity (EoP, via intraperitoneal IL-1β injection) and germinal matrix haemorrhage (GMH, via intraventricular collagenase VII injection). EoP and GMH were studied in independent animal cohorts; no subject received both models. We screened the route of administration (intranasal, IN versus intravenous, IV), dose (20, 50 and 125 M cells per kg bodyweight), and timing of delivery (acute, P5; secondary, P10; and tertiary, P20). Outcome measures are RNA sequencing and analysis of microtubule-associated protein (MAP2) and myelin basic protein (MBP) via western blotting or immunohistochemistry

animals were housed with a 12-h light/dark cycle and free access to food and water.

Inflammation-associated EoP

Wistar Han strain rats were purchased from Charles River (L'Abresle, France). Rats were intraperitoneally (i.p) injected twice daily from the post-natal day (P)1 to P4 and once in the morning of P5 with 10 µL recombinant mouse IL-1β (Miltenyi Biotec, Bergisch Gladbach, Germany) diluted in 1X PBS (0.12 M) to a final dose of 20 µg/kg, or the same volume of 1X PBS [44, 45, 49]. Separation from the dam was no more than five minutes per injection. Sex determination was performed at birth and confirmed at tissue collection. Male pups were used, as only males develop a consistent hypomyelination phenotype in this paradigm, reflecting the clinical scenario of a male bias to injury [50]. All litters were culled to 12 pups from P1 by random selection after sex determination.

Germinal matrix haemorrhage

Wistar Han rats were sourced from Janvier Labs and bred at the Experimental Biomedicine Centre, University of Gothenburg. Male and female rat pups were randomly allocated into control and GMH groups at P5. Following anaesthesia with isoflurane (5% for induction and 3.5% for maintenance) in a 1:2 mixture of oxygen and nitrogen, rats were injected in the right striatum with either collagenase VII (0.3 U, 1000–3000 CDU/mg solid, C2399, Sigma-Aldrich, Saint Louis, U.S.A.) to induce GMH or with PBS as control. Injections were administered at 1 µL per minute for 2 min into the right hemisphere, 1 mm rostral of the bregma and 4 mm lateral of the midline, and 3.5 mm in depth, using a 27G (0.4 mm diameter) needle attached to a 1 mL Hamilton syringe (Hamilton Company, Bonaduz, Switzerland) connected to an CMA 100 microinjection pump (CMA Microdialysis, Massachusetts, U.S.A) as described previously [34, 35, 47]. After recovery on a heating pad at 37 °C, pups were returned to their home cages. The duration of the procedure did not exceed five minutes per animal.

HuMSC culture

HuMSCs were supplied by Chiesi Farmaceutici after manufacturing by Lonza and were prepared according to the supplier's recommendations. Two days before administration, 5×10^6 cells were thawed at 37 °C, resuspended in complete medium (basal proprietary medium, complemented with 5% platelet lysate and 2000 U/L heparin), plated in T75 cell culture flasks (Corning, New York, U.S.A) and cultured for 48 h. HuMSCs were counted using the NC-200 cell counter (Chemometec, Allerød Denmark) and plated at 15×10^6 cells/mm^2 in T75 flasks. On the day of administration, cells were trypsinised (trypsin/EDTA 0.25%, Gibco, Munich, Germany), centrifuged (300 g × 3 min), and the cell pellet resuspended in cold, sterile PBS and counted. An additional cell count was performed immediately before administration.

Administration of the HuMSCs

We define the control (Ctrl) uninjured group as the PBS-treated (sham treatment) animals not subjected to injury, the injured group as IL-1β-exposed or GMH animals that did not receive a HuMSCs injection but received PBS (sham treatment), and the treated group as IL-1β-exposed or GMH animals that received a HuMSCs treatment (diluted in PBS). In the EoP model, 18 treatment protocols were tested: three different doses (20 M cells/kg, 50 M cells/kg, and 125 M cells/kg); three different time points (acute phase at P5, the subacute phase at P10 and the tertiary phase at P20); and two routes of administration [38] (IN versus IV). In the GMH model 8 treatment protocols were tested (IN and IV administration at P10 and P20, of 20 and 50 M cells/kg BW).

Magnetic-activated cell sorting and RNA extraction

Rats were anesthetised 48 h after HuMSCs administration with an i.p injection of pentobarbital sodium and phenytoin sodium (150 mg/kg, Euthasol, Virbac AH, Inc., Fort Worth, U.S.A) and intracardially perfused with 0.9% sodium chloride. The olfactory bulbs and cerebellum were removed, and remaining tissues dissociated using the Miltenyi Biotec Neural Tissue Dissociation kit (for P7 brains) or Adult Brain Dissociation kit (P12 and P22 brains), on the gentleMACS Octo Dissociator with heaters as per the manufacturers' instructions. From the resulting brain homogenate, microglia were enriched using anti-CD11b/c antibody-coupled microbeads (Miltenyi Biotec). After collection of the CD11b/c positive cell fraction, the isolated cells were centrifuged, and cell pellets were conserved at −80 °C until messenger RNA (mRNA) extraction. RNA was extracted using the NucleoSpin RNA XS Plus kit (Macherey–Nagel, Dueren, Germany) according to the manufacturer's recommendations and eluted in 16 µL of RNase-free water. Each protocol had $N = 3$ replicates; see Supplementary Table 1 for an overview of sequencing batches and replicates. RNA quality was assessed using an Agilent fragment analyser (5300 Fragment Analyzer System), and all samples were > 7 cutoff.

Library preparation, sequencing, and differential analyses

Library preparation and Illumina sequencing were performed at the Ecole Normale Superieure genomics core facility (Paris, France). Messenger (polyA +) RNAs were purified from 100 ng of total RNA using oligo(dT). Libraries were prepared using the strand-specific

RNA-Seq library preparation TruSeq Stranded mRNA kit (Illumina). Libraries were multiplexed by 15 on six flow cell lanes. A 75 bp single read sequencing was performed on a NextSeq 500 device (Illumina). An average of 27 ± 7 M reads passing the Illumina quality filter was obtained for each sample. Analyses were performed using the Eoulsan pipeline [51], including read filtering, mapping, alignment filtering, read quantile normalisation, and differential analysis. In the Eoulsan pipeline, reads were aligned against the rnor6 genome from Ensembl version 96 using STAR (version 2.7.2d) [52]. Then, alignments from reads that matched more than once on the reference genome were removed using samtools (Java version) [53]. We used the rnor6 GTF genome annotation version 96 from the Ensembl database to compute gene expression. All overlapping regions between alignments and referenced exons were counted and aggregated by gene using HTSeq-count 0.5.3 [54]. Finally, normalisation of sample counts, statistical treatments, and differential analyses were performed using DESeq2 1.8.1 [55]. The RNASeq gene expression data and raw fastq files are available on the GEO repository (www.ncbi.nlm.nih.gov/geo/) under accession number: GSE298271.

Signalling pathways analysis from RNAseq data

Heatmaps were generated using the Morpheus software (https://software.broadinstitute.org/morpheus), a hierarc hical clustering method that couples means using Pearson's correlation. The various gene functional annotations shown in the figures for each gene cluster were obtained by running an Over Representation Analysis (ORA) using WebGestalt (functional database: Gene Ontology, enrichment categories: Biological Process no Redundant, Molecular Function no Redundant, Cellular Component no Redundant, number of genes in category: between 5 and 2,000, FDR adjusted using Benjamini-Hochberg (BH) method with cut-off at 25%). For each cluster, the considered gene list comprises the genes within the cluster, and the background list consists of the measured genes in the corresponding RNA sequencing data.

In silicoefficacy scoring of RNA-sequencing data

The code required for this process is provided as supplementary data and is updated on a GitHub repository (https://github.com/INSERM-U1141-Neurodiderot/premstem-scoring).

Building a signature of HuMSC-induced treatments

A signature $s\rightarrow$ from reference group G_i (injured) to treated group G_t (that we denote $[G_i \rightarrow G_t]$) is a vector of numbers. $s\rightarrow$ is defined as a quantitative summary of differential gene expression analysis on treated group Gt compared to reference group Gi:

- The number of values in the signature is the number of significantly differentially up-regulated or down-regulated genes in treated group G_t compared to samples from reference group G_i.
- The positive (resp., negative) signs of these values correspond to up-regulation (resp., down-regulation).
- The absolute values of these coefficients correspond to the magnitude (or strength) of change in expression and are analogues to $\log_2$ fold changes.

Genes that are absent from the signature are either unaffected or non-significantly affected by the treatment (that is, their magnitude in the signature is equal to zero). Conversely, genes associated with nonzero coefficients in the signature are significantly altered genes. Thus, the signature $s\rightarrow$ accounts for both the direction and the magnitude of changes in gene expression for each gene. Here, we consider the microglial change from the injured group to control or from injured to treated groups, which belong to the same sequencing batch (Supplementary Table 1). To build signatures, let us first notice that classical differential expression analyses are usually performed independently for each gene (univariate differential analyses). However, the transcriptomic impact of a treatment is often driven by groups of genes that may individually carry low changes in expression. To consider group-of-genes effects on expression, we used Characteristic Direction (CD) to compute $s\rightarrow$ [56] (Supplementary Fig. 1 and Fig. 2). First, for a given sequencing batch (associated with a fixed route and age of administration), we considered its normalised expression matrix as provided by DESeq2 (Supplementary Table 2) [55]. Then, for each group (injured or treated), we only preserved samples in the matrix that belonged to either the treated or injured groups. Then, we applied the Characteristic Direction procedure to this matrix to determine the classification frontier between the treated and injured groups. This frontier is a high-dimensional vector with a number of coefficients equal to the number of genes. It roughly splits samples into two parts of the high-dimensional plane, each corresponding to one of the conditions. This vector is computed by performing a type of regression called Linear Discriminant Analysis (LDA) on the gene expression matrix. Second, from the frontier determined at the first step, we computed vector $s\rightarrow$, characterised by its direction and norm, such that $s\rightarrow$ is orthogonal to the frontier, goes from the control group Gi to the treated group Gt, and its coefficients V_1, V_2, … V_N satisfy the equation $V_1^2 + V_2^2 + \ldots V_N^2 = 1$, where N is the total number of genes measured in the dataset (Supplementary Fig. 1a). Note that, as shown in (Supplementary Fig. 1b), coefficient V_1 (resp. V_2, … V_N) is the

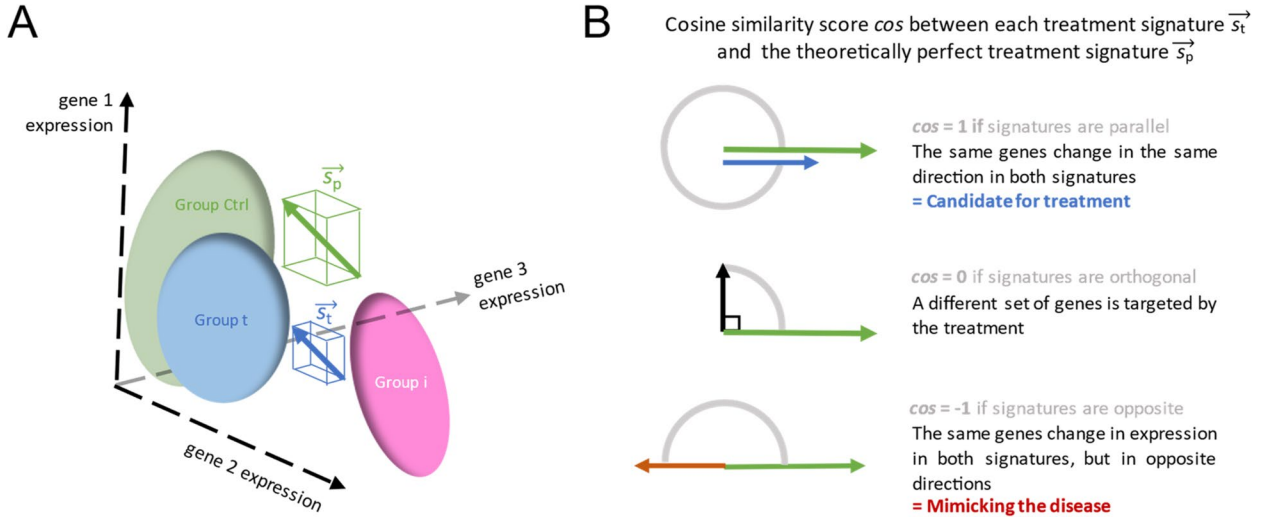

Fig. 2 Overview of the scoring pipeline. **A** Projection of transcriptome data in geometrical gene expression space and creation of vectors of characteristic direction (CD) signatures between injured (i), treated (t), and control (Ctrl) groups. **B** Representation of the extreme values of the cosine score *cos* quantifying the similarity between two signatures (*s*). Here, to rank the various HuMSC treatment paradigms, the score *cos* was computed to compare the treatment *t* protocol overall impact on gene expression (s_t) with a theoretically perfect treatment signature (s_p)

projection of signature $s \rightarrow$ onto the axis associated with the first (resp., second, … N^{th} gene of the list; its absolute value grows as the gene expression is greatly affected by the treatment; and goes in the direction of the increasing (resp., decreasing values on the axis if the gene is up-regulated (resp., down-regulated by the HuMSC treatment. Using this procedure, we then compute the theoretically perfect treatment signature $s_p \rightarrow$ [injured → control] and all tested experimental protocols signatures: $s_1 \rightarrow$ [injured → Dose 1-treated], $s_2 \rightarrow$ [injured → Dose 2-treated], $s_3 \rightarrow$ [injured → Dose 3-treated].

Design of the scoring process for ranking HuMSC efficacy

The treatments were then ranked according to their ability to reverse injury-induced changes in gene expression based on the signatures computed as described in the previous section. For each treated group (Dose *i*-treated) in each sequencing batch, we computed the cosine similarity score (denoted *cos*) between its associated signature [model → Dose *i*-treated] and the corresponding theoretically perfect treatment signature [injured → control] (Fig. 2B). The computation of score *cos* (s_1, s_2) for any pair of signature vectors s_1 and s_2 (both of length n and where s^i is the ^{i}th coefficient of vector *s*) is score *cos* ([injured → Dose *i*-treated], [injured → control]). The score is between −1 and 1. The closer this score is to 1, the more similar the microglial transcriptome to the treated group at Dose *i* are to the control group. Therefore, HuMCSs at Dose *i* restored a normal microglia transcriptional profile. Note that treatments that yield a score close to −1 (and, generally, any negative score) reflect no improvement in the changes in microglial gene expression from the injury-only group.

Protein extraction and western blotting

Snap-frozen right anterior cortex from the mice was homogenised in RIPA Buffer (Sigma-Aldrich) containing protease inhibitors (cOmplete Tablets, Roche, Basel, Switzerland) in gentleMACS M tubes using a gentleMACS dissociator (Miltenyi Biotec) as per the manufacturer's instructions. The samples were centrifuged (10,000 g, 10 min, 4 °C), the supernatants were collected and centrifuged again, and the pellets were stored for later use. Equal amounts of protein (25 µg), as determined by BCA protein assays (Sigma-Aldrich), were diluted with Lamemli sample buffer (Biorad, Basel, Switzerland) containing 2-mercaptoethanol (Sigma-Aldrich) and then separated in Mini-protean TGX gels (Any kD, Biorad; 80 V for 110 min). Proteins were then electrotransferred (Trans-blot Turbi, Biorad) onto a 0.2 µm nitrocellulose membrane (Trans-Blot Turbo Transfer Pack, mini, Biorad). Based on the predicted molecular weight of our target proteins and using a ladder marker as a guide, the membrane was cut into an upper and lower portion, and both were incubated in a blocking solution (5% bovine serum albumin, 0.1% Tween 20 in TBS) for one hour. Then, the lower portion was incubated with mouse anti-b-actin (Sigma-Aldrich AC-74, 1:20,000) and the upper portion with rat anti-MBP (Millipore MAB386 1:500) overnight at 4 °C in blocking solution. Blots were rinsed with 0.1% Tween 20 in TBS and incubated for one hour with an HRP-conjugate goat anti-mouse IgG (1:2,000; Sigma-Aldrich) or HRP-conjugate goat anti-rat IgG (1:10,000; Invitrogen) in blocking solution. The blots were washed three times with 0.1% Tween 20 in TBS for five minutes. Membranes were processed with the Clarity Western ECL substrate (Biorad), and the proteins of

interest were investigated with Syngene PXi (Syngene) coupled to acquisition software. The immunoreactivity of four isoforms of MBP was compared with that of actin controls using NIH image J software (2.0.0-rc-44/1.50e, http://rsb.info.nih.gov/ij/).

MAP2 and MBP immunohistological analyses

Rats were anesthetised by i.p injection with pentobarbital, perfused with 5% buffered formaldehyde (Histofix, Histolab, Askim, Sweden), then the brains were collected and stored at 4 °C in Histofix overnight before paraffin-embedding. Coronal sections of the forebrain were cut at 7 µm. Staining for MAP2 was performed on every 50th Sect. (6 sections/animal) and for MBP on every 100th Sect. (3 sections/animal). Briefly, the sections were deparaffinised, followed by heat-mediated antigen retrieval in 0.01 M citric acid and peroxidase blocking in 3% H_2O_2 in 0.1 M phosphate buffer. After non-specific antibody blocking with 4% bovine serum albumin (BSA), sections were incubated with mouse anti-microtubule-associated protein 2 (MAP-2, 1:1,000 dilution; M4403, Sigma-Aldrich, United States), mouse anti-myelin basic protein (MBP, 1:1,000 dilution; SMI-94 Covance, Princeton, U.S.A) overnight at 4 °C. The following day, the sections were incubated with the corresponding secondary antibodies (1/200, Vector Labs, Burlingame, CA, United States) for 1 h at room temperature. The sections were then incubated for one hour in ABC Elite (Vector Labs) and visualised via incubation in 0.5 mg/ml 3.3-diaminobenzidine in a buffer consisting of $NiSO_4$, β-D-glucose, NH_4Cl, and β-D-glucose oxidase (all from Sigma-Aldrich).

Automated quantitative analysis of brain injury using machine-learning

Images were acquired using a Zeiss Axioscan 7 slide scanner and quantified using ZEN Blue (3.2) software. Automated image segmentation was performed using a machine learning approach with Zen Intellisis. Two different Intellesis segmentation models were created by training on several images selected from all groups with varying staining intensity: (1) a model for segmentation of MBP positive areas in the striatum, and (2) a model for segmentation of MAP2 fibres in the motor cortex. These models were used to segment and quantify all images. An interactive measurement using these models was performed by defining a region of interest (ROI) in the striatum and motor cortex. The striatum ROI was determined by manually drawing around the entire striatum (Supplementary Fig. 2). To quantify MAP2 positive fibres in the cortex, a custom ROI of dimensions 2905.57 um by 1452.78 um was applied to all images in the M2/M1 region of the motor cortex (Supplementary Fig. 2). Following automated machine learning-based segmentation, the MAP2 positive area in the striatum, MAP2 fibre count, length, and area coverage were quantified.

Statistics

The primary purpose of analysing the Western blotting data from the EoP was to determine the overall effects of injury and treatment on the group means, which was achieved using a Kruskal–Wallis test, as the data were not normally distributed. The second purpose was to determine which treatment applied in a trial would have caused significant changes in myelin content, and this was achieved using an uncorrected Dunn's test comparing groups to the injury condition. Similarly, for the analysis of MBP and MAP2 in the GMH model, an ANOVA was first applied to determine the overall effect of injury and treatment on group means. Subsequently, to assess the specific impact of treatment on the outcome measure, multiple comparisons were made with the injury condition, adjusting for a false discovery rate (FDR) of 0.05 using the Benjamini, Krieger, and Yekutieli method, as the comparisons are not independent. Our multiple comparison tests are valid even in the absence of a significant ANOVA, given these analysis goals and the chosen tests. The analysis of the RNAseq data is described above.

Results

Model 1 — inflammation-associated encephalopathy of prematurity (EoP)

Validation of the impacts on the microglial transcriptome in the inflammation-induced model of EoP

In this model of EoP, systemic inflammation is induced by postnatal day (P)1–5 intraperitoneal interleukin-1β injection which induces neuroinflammation, which leads to oligodendrocyte maturation arrest, hypomyelination, interneuronopathy, and deficits on MRI and in behaviours [44, 46]. We have studied the microglia reactivity profile in this model in detail in the mouse in the acute and subacute phases (between P1-P10) and found a combined immune-reactivity and disruption to developmental and homeostatic functions [19, 57]. In this study, our first goal was to verify this microglia reactivity profile in the rat at P7 and characterise the novel time points of P12 and P22. In the sub-acute stages of injury in this model, at P12, the rat brain is approximately equivalent to that of an infant in the first month of life. In the tertiary phase of injury in this model, at P22, the rat brain is approximately equivalent to brain development in a 3-year-old child. We previously described that more than 95% of positive cells in our systemic inflammation-induced EoP paradigm applied to mice are microglia [57]. Similarly, in the rat, we observed that 95 + % of CD11b/c isolated cells were microglia, wherein we defined microglia as $CD11b^{hi}$ $CD45l^{o}$ cells, neutrophils defined as $CD11b^{hi}$ $CD45^{hi}$ $Ly6G^{hi}$, monocytes defined as $CD11b^{hi}$ $CD45^{hi}$

$Ly6G^{lo}$ $F4/80^{lo}$ cells and macrophages defined as $CD11b^{hi}$ $CD45^{hi}$ $Ly6G^{lo}$ $F4/80^{hi}$ cells using fluorescent activated cell sorting. As such, we isolated CD11b/c positive microglia using our well-established paradigm [19, 49, 58] and subjected them to RNA sequencing and analysis. The treatment, N, and batch summary are in Supplementary Table 1.

Using a traditional univariate approach (DESeq2), 945 genes were significantly differentially altered (Benjamini-Hochberg (BH) adjusted p-value < 0.05) under at least one control (PBS only, uninjured) or IL-1β (injured) condition at P7, P12 or P22 (Supplementary Table 2). Clusters generated using Morpheus (https://software.broadinstitute.org/morpheus) (Fig. 3a) were annotated using the Gene Ontology database integrated into DAVID 6.8 (Fig. 3b), and the annotations of the impacts of systemic inflammation were generally in agreement with our previous analysis of microglia in this model [19, 57, 59]. Comparing the injured and control groups, we observed two clusters at P7: Cluster A and Cluster B. The genes comprising Cluster A were more highly expressed in control animals and included those related to the cell cycle. Genes making up Cluster B were more highly expressed in injured animals and involved response genes to an inflammatory stimulus, signal transduction and cell death. A third cluster, Cluster C, was expressed by uninjured (PBS control) and injured (IL-1β-exposed) at P7 and P22 and is populated with genes associated with immune responses.

Ranking of the efficacy of HuMSC treatments in a model of inflammation-induced EoP

The vast amount of data outputs from transcriptomics and well-defined analysis pipelines make sequencing approaches valuable in developing a deep understanding of specific events in small groups. However, these traditional methods are not well-suited to analyse the 18 groups in this study to address the question of which time (acute, sub-acute, tertiary), treatment dose (20, 50, 125 M

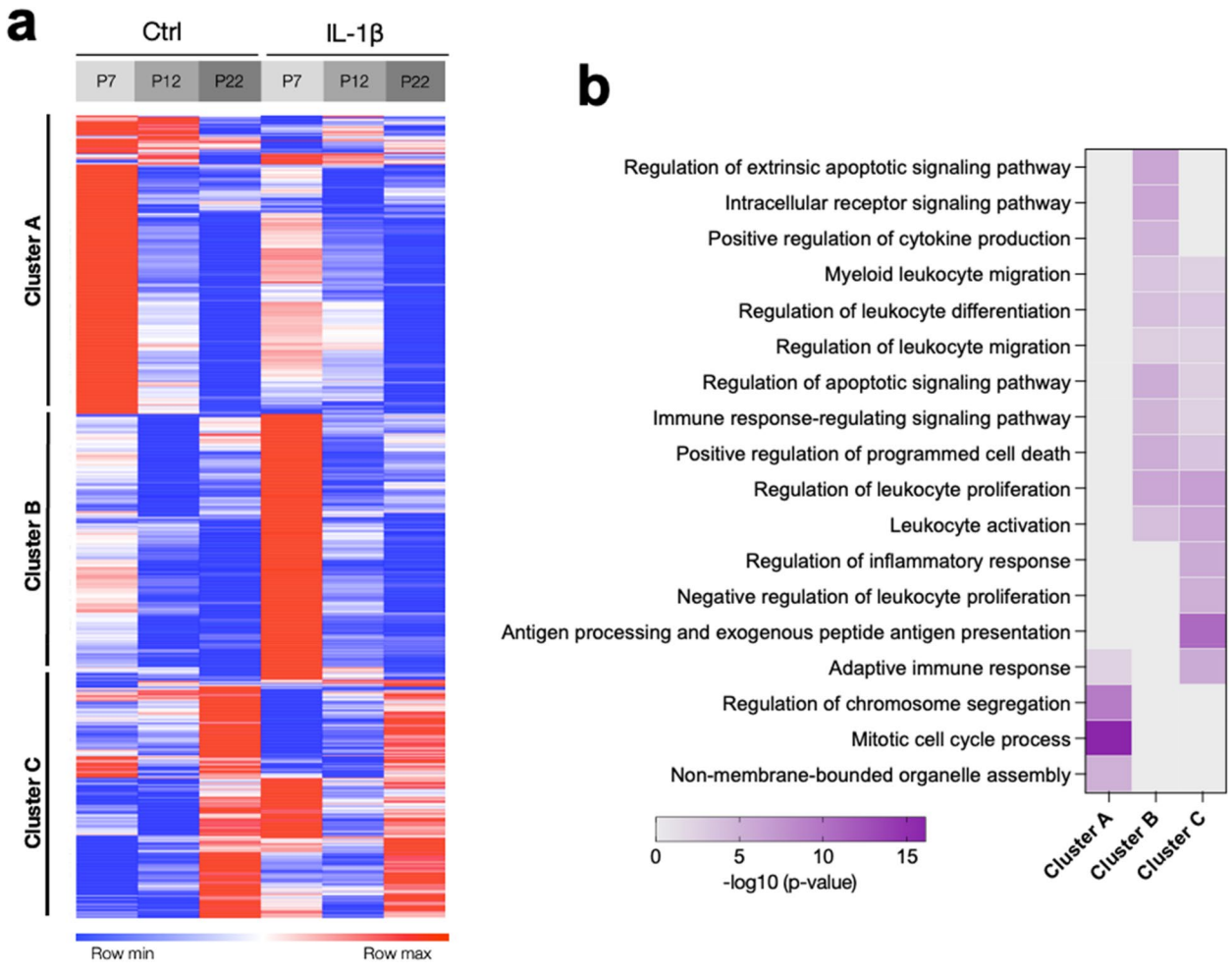

Fig. 3 EoP model: The effects of exposure to IL-1β from P1-P5 on the microglial transcriptome were assessed using RNA sequencing. In **a** clusters of genes that were differentially expressed between Control (Ctrl) and cells from IL-1β exposed rats (Benjamini–Hochberg adjusted p-value < 0.05) were visualised. In **b** these clusters were annotated using a gene ontology analysis (DAVID 6.8) to reveal impacts on inflammatory processes and proliferation

cells/kg BW), and administration route (IN vs IV) is the most neuroprotective. We established a unique screening pipeline to address this challenge. Firstly, we used a multivariate approach called Characteristic Direction (CD), which is more sensitive and more robust than traditional univariate approaches, to identify differentially expressed genes, particularly in response to treatment perturbation [56]. We considered the transcriptome profiling of control animals (injected with PBS only) as the ideal healthy state to retrieve through the MSC treatment and the transcriptome profiling of injured animals (injected with IL-1β only) as the reference injured state to compare each treatment option. The expected treatment response was estimated by computing the CD between these two states (control and injured). We also computed CD for the 18 treatment options. For each option, the similarity between the expected and the treatment response CDs was evaluated by measuring the angle between these two directions, a natural distance measurement called the Cosine score (Supplementary Fig. 1 and methods). This score is a value between −1 and 1.

This score represents how similar the two biological comparisons are. The closer the score is to one, the closer the treatment response looks like retrieving a healthy state from the injured state – indicating that the HuMSC treatment has prevented the changes in the transcriptional landscape caused by injury. The results of the first stage of our scoring system are in Table 1. There were no sequencing batch effects on the scores. Most of the scores are positive, indicating positive impacts of the HuMSC treatment on the injury-related transcriptome. The highest score was 0.8 for the intranasal treatment protocol initiated at P20 using 50 M cells/kg. Treatments via the intranasal route consistently ranked higher than IV treatments, with 4 out of 5 top scores being intranasal and only 1 out of 5 lowest scores being intranasal treatments. There was no monotonic (dose-dependent) effect on the score. For interest, we created a cluster map of the differentially expressed genes (BH, $P<0.05$) for the group with the highest ranking (0.80, IN treatment at P20 with 50 M cells/kg BW, Fig. 4a) to explore preliminarily the pathways modulating the positive association (Fig. 4b). Interestingly, only one pathway related to inflammation in Cluster A, 'Response to dsRNA', but the others are primarily related to homeostasis and cell stress responses. Cluster B had no direct links with inflammation, and all pathways were linked to fundamental structural development.

Table 1 EoP model. Summary of Cosine score by treatment group

	Cosine score	Age at treatment	Mode of delivery	Dose
TOP RANKED	0.8	**P20**	**IN**	50M
	0.79	P10	**IN**	125M
	0.68	*P5*	**IN**	*20M*
	0.55	**P20**	IV	*20M*
	0.54	*P5*	**IN**	50M
	0.51	**P20**	**IN**	125M
	0.36	P10	**IN**	*20M*
	0.33	P10	**IN**	50M
	0.31	*P5*	**IN**	125M
	0.27	**P20**	IV	125M
	0.24	P10	IV	*20M*
	0.2	**P20**	IV	50M
	0.11	*P5*	IV	125M
BOTTOM RANKED	0.08	**P20**	**IN**	*20M*
	0.08	P10	IV	50M
	0.01	P10	IV	125M
	-0.02	*P5*	IV	*20M*
	-0.12	*P5*	IV	50M

Completion of the ranking by analysis of myelination in a model of inflammation-induced EoP

Exposure to systemic and neuroinflammation from P1-5 recapitulates the clinical phenotype of white matter injury, which is driven by a blockage of oligodendrocyte maturation and a decrease in the production of myelin proteins [60, 61]. Thus, measuring the expression of MBP was used as the second component of the scoring system to measure the neurotherapeutic efficacy of the HuMSCs. MBP was assessed via western blotting (Fig. 5). We analysed whether the means of the MBP data varied between groups for each time point of treatment using a Kruskal–Wallis test (Table 2; the P10 and P20 analyses were significant ($p<0.002$. We also applied an uncorrected Dunn's multiple comparison test using the IL-1β group as the comparison to detect specific treatment effects. The data are shown in Fig. 5.

Specifically, we found that exposure to IL-1β from P1-5 significantly altered the expression of MBP at P12 (Fig. 5c, decreased 31%, $p=0.0027$) and P22 (Fig. 5d, decreased 19%, $p=0.0565$). However, at P7, when MPB expression is still relatively low, although mean expression was reduced by 15%, this was not significant (Fig. 5b, $p=0.182$). Considering HuMSC effects, in the acute phase treatment paradigm, at P5, we observed that there were no increases in MBP with HuMSC treatment, and 20 M cells/kg IN treatment tended to decrease MBP (Fig. 5b, by 27%, $p=0.0814$). In the sub-acute treatment paradigm, applied at P10, there was a significant increase in MBP compared to IL-1β only in the 20 and 125 M cells/kg groups treated IV and in the 50 M cells/kg group treated IN (Fig. 5c). In the delayed treatment, applied at P20 in the tertiary phase, IV treatment had no positive effects at any dose. In contrast, there was a significant

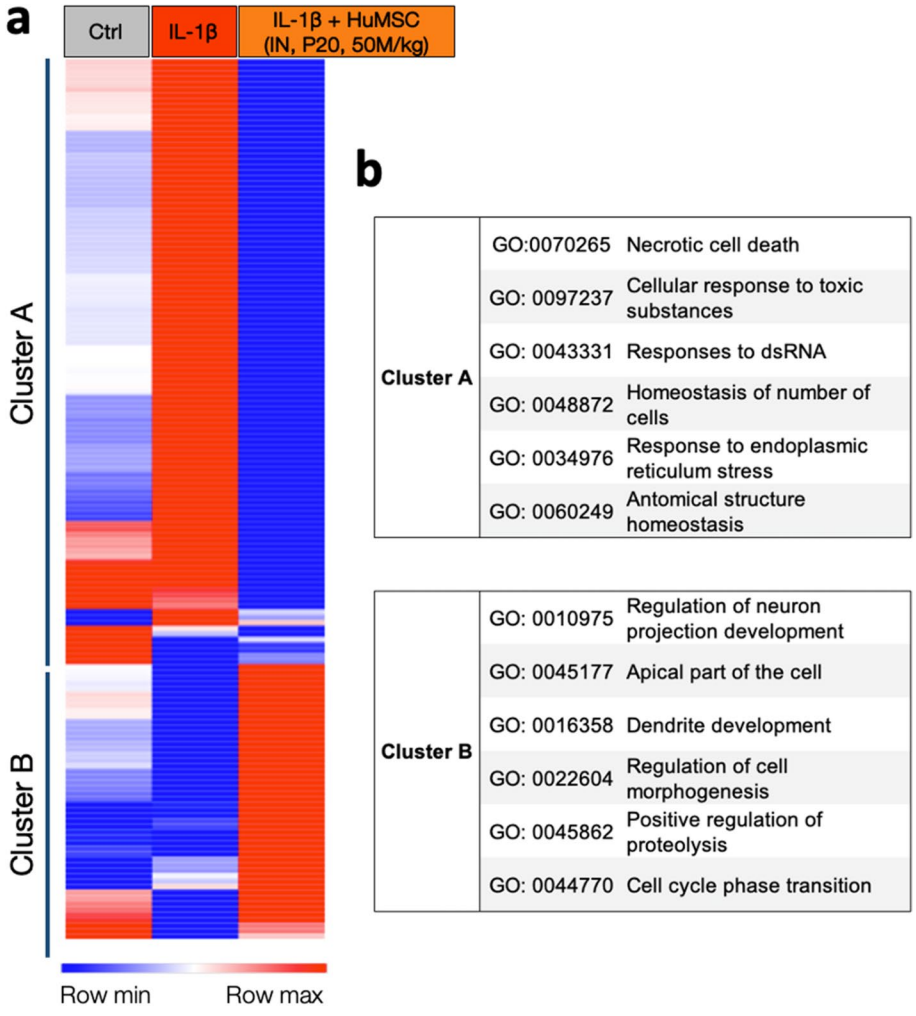

Fig. 4 EoP model. Analysis of differentially expressed genes in the top-ranked treatment group (0.80 score: IN treatment at P20 with 50 M cells/kg) illustrating in **a** gene clusters and in **b** the mapped gene ontologies

increase in MBP compared with IL-1β only mediated by IN MSC treatment at all doses (Fig. 5d).

We then brought together the two data sets, to create the scoring matrix. We directly compared the Cosine score and the impact on MBP (Fig. 5e). We found that highest Cosine score was the P20 IN 50 M cells/kg which significantly increased MBP, by approximately 60%. Overall, IN treatments had higher Cosine scores, and two of the three tertiary phase treatments were in the top Cosine scores.

Model 2 — Germinal matrix haemorrhage (GMH)

Validation of ranking by decrease of brain injury in the GMH model

To verify the ability of our composite microglia transcriptome and myelin protein scoring system to identify neurotherapeutic HuMSC treatments, we undertook further testing of the HuMSC efficacy in a rat model of GMH. We tested HuMSC efficacy via IN delivery at sub-acute (P10) and tertiary (P20) treatment paradigms at 20 and 50 M cells/kg BW, analysing neuronal microtubule-associated protein 2 (MAP2) and MBP (Supplementary Figs. 3 and 4, Figs. 6 and 7, and Table 3). We excluded the P5 paradigm and 125 M cells/kg, as these had no positive or negative impacts on outcomes in the first-line screen (Table 2, Fig. 5). As such, we assessed four paradigms of treatment: (1) 20 M cells/kg BW delivered five days after GMH at P10, with the injury assessed ten days later at P20, (2) 20 M cells/kg BW delivered fifteen days after GMH at P20, with the injury assessed ten days later at P30, (3) 50 M cells/kg BW delivered five days after GMH at P10, with the injury assessed ten days later at P20 and (4) 50 M cells/kg BW delivered fifteen days after GMH at P20, with the injury assessed ten days later at P30. To assess the overall impacts of injury and treatment, the control (ctrl; uninjured), GMH (with PBS vehicle treatment), and GMH + HuMSC (in PBS vehicle) groups were compared using a One-Way ANOVA, as they passed the

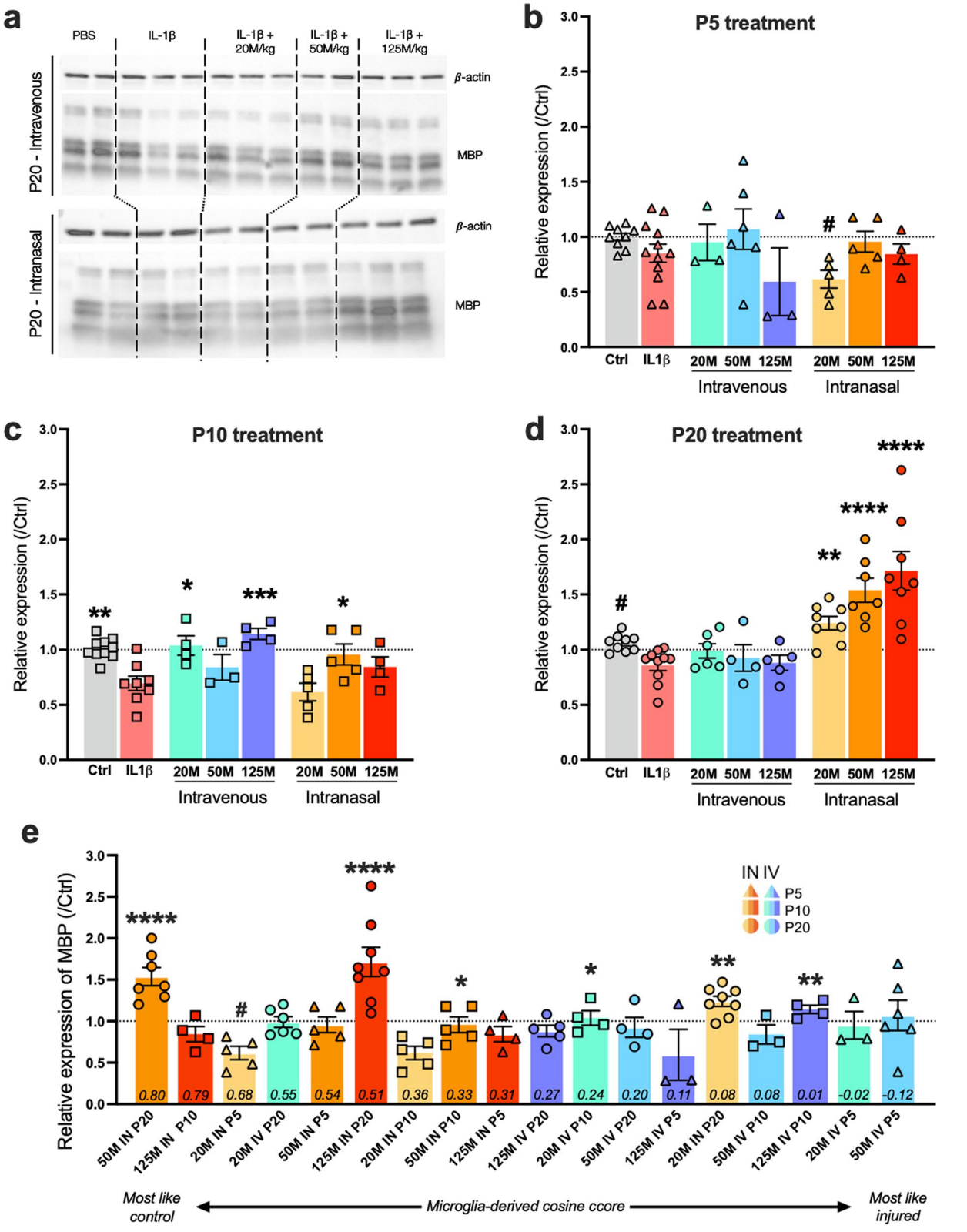

Fig. 5 EoP model. Analysis of expression of MBP across groups following HuMSC treatment. In **a** example blots from treatment at P20, and analysis following treatment at **b** P5, (**c**) P10 and **d** P20 analysed with a Kruskal–Wallis test and Dunns multiple comparison testing. In **e** a summary of the MBP data arranged in left to right order of highest to lowest microglial cosine score (from Supplementary Table 2). The cosine score is presented in italics in the bottom of each bar

Table 2 Main effects statistical outputs from the EoP model

Output, age: test	Figure	Main effects statistics
MBP frontal cortex, P5: Kruskal–Wallis	Fig 4b	H (7, 47) = 10.93, $p = 0.1417$
MBP frontal cortex, P10: Kruskal–Wallis	Fig 4c	H (7, 43) = 23.57, $p = 0.0014$
MBP frontal cortex, P20: Kruskal–Wallis	Fig 4c	H (7, 57) = 39.58, $p = < 0.0001$

Brown-Forsythe test (reported in Table 3). The specific changes from GMH were assessed with an FDR correction to 5%; q values are reported on Supplementary Figs. 3 and 4 and Figs. 6 and 7.

We first assessed MAP2 loss in the striatum and the effects of IV delivery for the four groups. Significant changes in the means across the groups were noted only in IV treatment with 20 M cells/kg at PND20 and IV treatment with 50 M cells/kg at PND10 (Table 3; Supplementary Fig. 3). In the multiple comparison testing, we only uncovered a non-significant trend (q = 0.063) for a HuMSC treatment effect for 50 M cells/kg at PND10 (Supplementary Fig. 3). No other analyses were undertaken for the IV groups based on this and the low ranking from the EoP model (Fig. 5e).

We then assessed the effects of IN treatments on MAP2 loss in the striatum (Fig. 6, Table 3). In the ANOVA, there was a trend toward change across group means for the IN treatment with 20 M cells/kg at PND20 ($p = 0.063$). The three other IN-treated groups reported significant differences across the means of the three groups (all, $p < 0.01$; Table 3). Specifically, in the multiple comparison testing, GMH led to a significant loss of MAP2, which was not recovered by 20 M cells/kg treatment at PND10 or PND20 (Fig. 6b,c). However, the loss of MAP due to GMH was significantly recovered by IN 50 M cells/kg at P10 (q = 0.039; Fig. 6d) and showed a trend toward recovery with IN 50 M cells/kg at PND20 (q = 0.057; Fig. 6e).

We then assessed the effects of GMH and HuMSC on loss of myelinated nerve fibres for the treatments found to have positive impacts on MAP2: 50 M cells/kg IN PND10 and PND20 (MBP expression, Supplementary Fig. 4, Fig. 6). When we delivered 50 M cells/kg IN five days after GMH (at P10) and evaluated injury on P20, we found no change in the group means for a total area coverage of MBP in the striatum (Table 3), similarly reflected

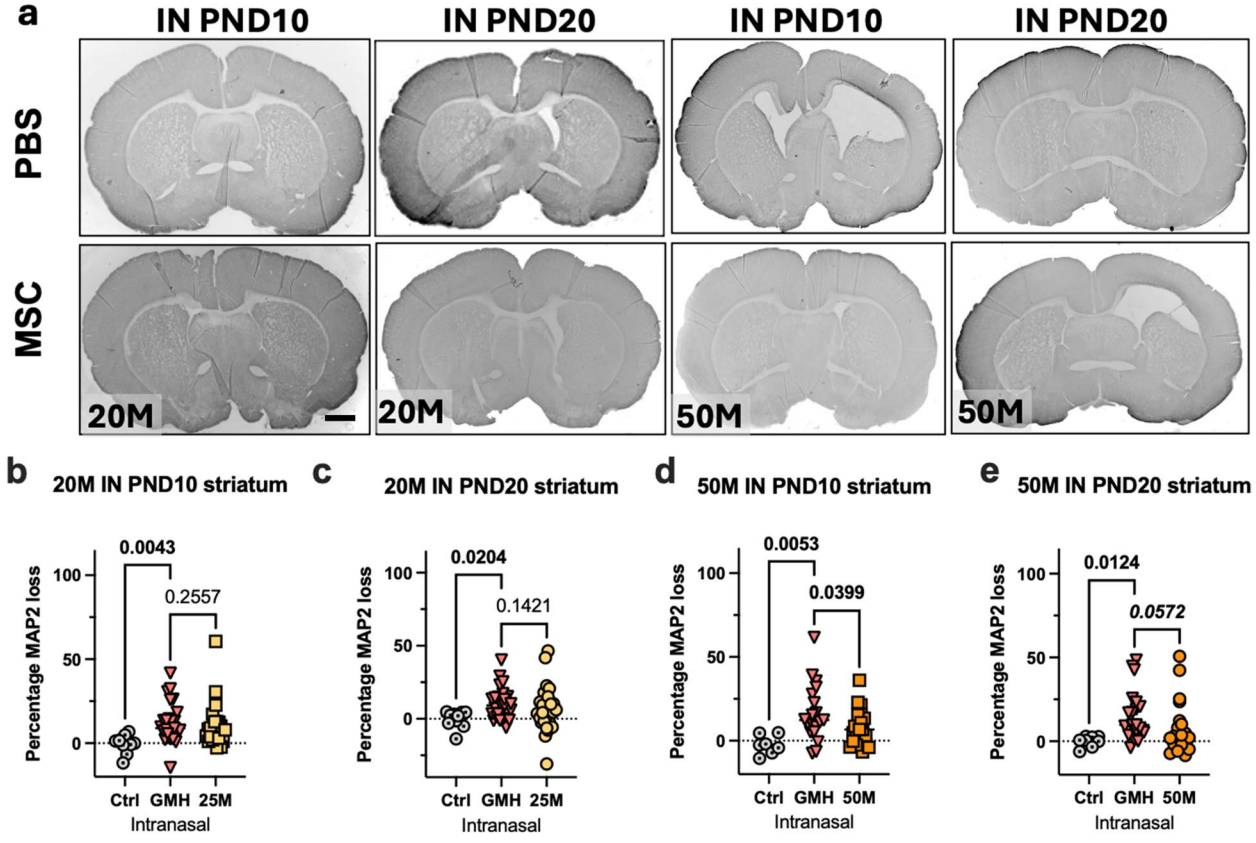

Fig. 6 GMH model. Effects of HuMSC treatment on a loss of MAP2 protein. In **a** example MAP2 striatal staining from control and GHM animals treated with 20 M cells/kg IN at PND10. Scale bar = 1 mm. Analysis of MAP2 loss in the pups treated with 20 M cells/kg IN at **b** PND10 and **c** PND20, then in the pups treated with 50 M cells/kg IN at **d** PND10 and **e** PND20. Analyses via a Kruskal–Wallis test (see Table 4) and results from the multiple comparison to GMH adjusted to a 5% FDR are shown

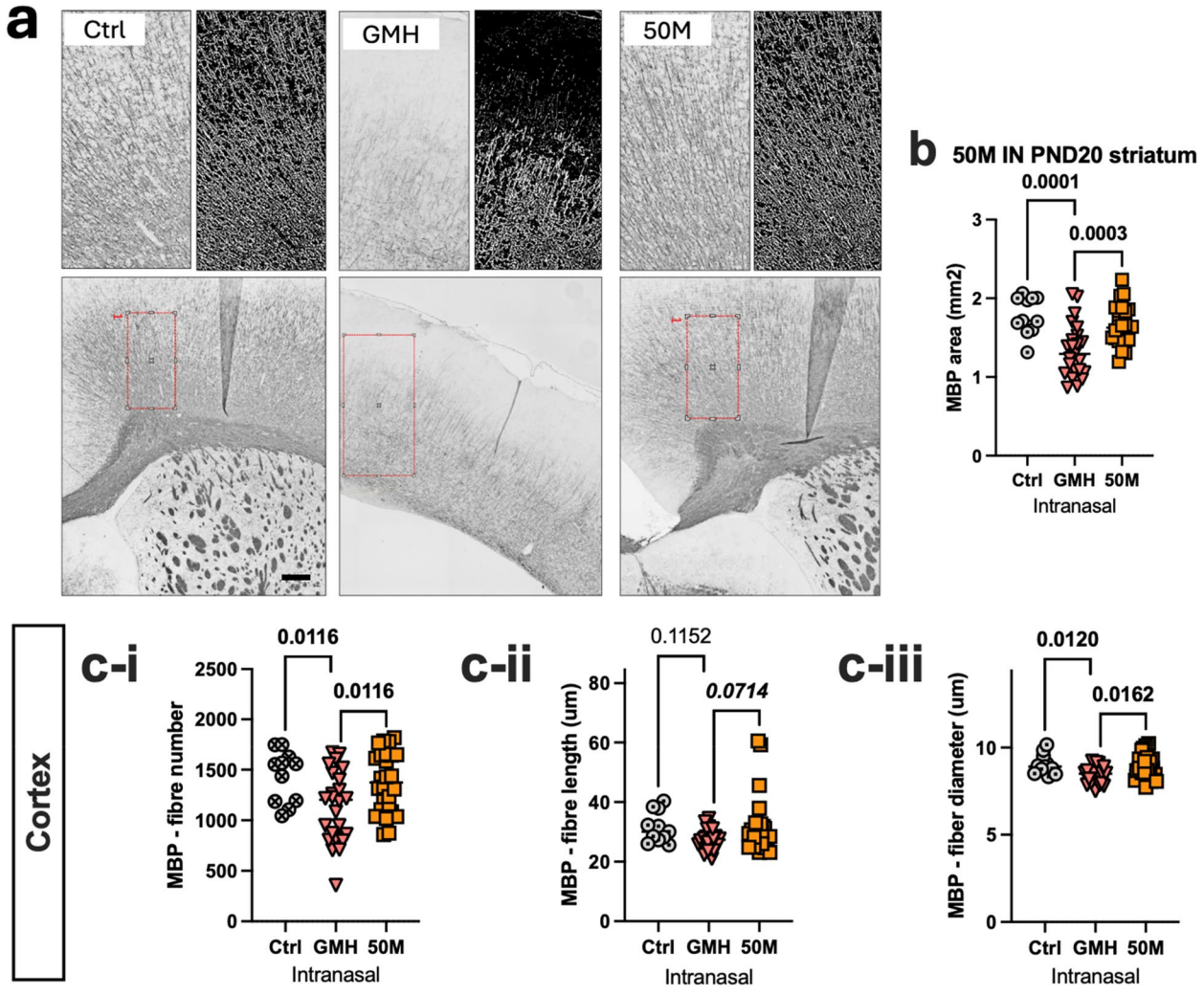

Fig. 7 GMH model. Effects of HuMSC treatment on expression characteristics of MBP. In **a** example MBP striatal staining from control and GHM animals treated with 50 M cells/kg, IN at PND20. Scale bar = 200um. Analysis of MBP in the pups treated with 50 M cells/kg IN at PND20, showing in **b** MBP area coverage in the striatum, and then in the cortex (c-i) MBP positive fibre number, (c-ii) MBP fibre length, (c-iii) MBP fibre diameter. Analyses as per Table 3 and results from the multiple comparison to GMH adjusted to an FDR of 5% are shown

with no group-specific changes (Supplementary Fig. 4a). There was a significant change in the group means for the outcome measures of MBP fibre length and diameter that were noted to be driven by injury effects from the GMH itself ($q < 0.01$) and not any effects of treatment ($q > 0.12$; Supplementary Fig. 4b).

We then tested the higher dose of 50 M cells/kg, administered 15 days after GMH (at P20), and evaluated injury on P30 (Fig. 7). In this paradigm, there were significant differences in the group means for MBP in the striatum and MBP characteristics in the cortex; fibre number and fibre diameter (Table 3). Specifically, the GMH induced reduction in MBP-positive white matter area of the striatum ($q = 0.0001$) was recovered by HuMSC treatment ($q = 0.0003$; Fig. 7a). When we looked at the specific characteristics of the MBP positive myelin in the cortex, HuMSCs significantly improved GMH-induced changes in MBP positive fibre number ($q = 0.011$) MBP positive fibre diameter ($q = 0.016$) and caused a non-significant trend to an increase in MBP positive fibre length ($q = 0.071$) (Fig. 7c).

Discussion

We developed a scoring system using indices of microglial gene expression changes and myelin protein expression to rank the efficacy of HuMSC treatments in a model of inflammation-induced EoP. This scoring system enabled us to screen 18 groups effectively and was predictive of treatment efficacy in a second brain injury model relevant to preterm-born infants. Across treatments and models, we found that HuMSCs at 50 M cells/kg BW, when administered in the tertiary phase (15 days) after injury via the IN route, were the most effective at reducing white and grey matter injury (Table 4, bold).

Table 3 Main effects statistical outputs from GMH model

Dose/Route/Treatment Age/Output/region: Test	Figure	Main effects statistics
20 M IV PND10 MAP2 loss striatum: One Way ANOVA	S. Fig 3a	H (2, 50) = 0.93, p = 0.401
20 M IV PND20 MAP2 loss striatum: One Way ANOVA	S. Fig 3b	H (2, 52) = 10.51, p = 0.0001
50 M IV PND10 MAP2 loss striatum: One Way ANOVA	S. Fig 3c	H (2, 52) = 11.46, p = 0.010
50 M IV PND20 MAP2 loss striatum: One Way ANOVA	S. Fig 3d	H (2, 46) = 2.08, p = 0.136
20 M IN PND10 MAP2 loss striatum: One Way ANOVA	Fig 5c	H (2, 58) = 4.61, p = 0.013
20 M IN PND20 MAP2 loss striatum: One Way ANOVA	Fig 5d	H (2, 61) = 2.89, p = 0.063
50 M IN PND10 MAP2 loss striatum: One Way ANOVA	Fig 5e	H (2, 44) = 5.63, p = 0.006
50 M IN PND20 MAP2 loss striatum: One Way ANOVA	Fig 5f	H (2, 44) = 3.70, p = 0.032
50 M IN PND10 MBP area cover striatum: One Way ANOVA	S. Fig 4a	H (2,48) = 1.613, p = 0.21
50 M IN PND10 MBP fibre number cortex: One Way ANOVA	S. Fig 4b-i	H (2,45) = 2.079, p = 0.137
50 M IN PND10 MBP fibre length cortex: One Way ANOVA	S. Fig 4b-ii	H (2,45) = 4.108, p = 0.023
50 M IN PND10 MBP fibre diameter cortex: One Way ANOVA	S. Fig 4b-iii	H (2,45) = 3.695, p = 0.037
50 M IN PND20 MBP area striatum: One Way ANOVA	Fig 6b	H (2,57) = 11.87, p = < 0.0001
50 M IN PND20 MBP fibre number cortex: One Way ANOVA	Fig 6c-i	H (2, 58) = 5.12, p = 0.0008
50 M IN PND20 MBP fibre length cortex: One Way ANOVA	Fig 6c-ii	H (2, 58) = 2.69, p = 0.076
50 M IN PND20 MBP fibre diameter cortex: One Way ANOVA	Fig 6c-iii	H (2, 58) = 5.18, p = 0.008

Table 4 At-a-glance efficacy map including EoP cosine and MBP findings, and GMH MAP2 and MBP findings

Route × Time	20 M/kg	50 M/kg	125 M/kg
IN P5	Cosine: 0.30 EoP MBP: ↓ GMH: n.t	Cosine: 0.25 EoP MBP: ↔ GMH: n.t	Cosine: 0.20 EoP MBP: ↔ GMH: n.t
IN P10	Cosine: 0.55 EoP MBP: ↔ GMH: MAP2: ↔; MBP: ↔	Cosine: 0.70 EoP MBP: ↑✓ GMH: MAP2: ↑✓; MBP: ↔	Cosine: 0.60 EoP MBP: ↔ GMH: n.t
IN P20	Cosine: 0.65 EoP MBP: ↑✓ GMH: MAP2: ↔; MBP: ↔	Cosine: 0.80 EoP MBP: ↑✓ GMH: MAP2: ↑•; MBP: ↑✓	Cosine: 0.72 EoP MBP: ↑✓ GMH: n.t
IV P5	Cosine: 0.10 EoP MBP: ↔ GMH: n.t	Cosine: 0.15 EoP MBP: ↔ GMH: n.t	Cosine: 0.12 EoP MBP: ↔ GMH: n.t
IV P10	Cosine: 0.40 EoP MBP: ↑✓ GMH: n.t	Cosine: 0.55 EoP MBP: ↔ GMH: n.t	Cosine: 0.50 EoP MBP: ↑✓ GMH: n.t
IV P20	Cosine: 0.35 EoP MBP: ↔ GMH: n.t	Cosine: 0.45 EoP MBP: ↔ GMH: n.t	Cosine: 0.38 EoP MBP: ↔ GMH: n.t

↑ increase; ↓ decrease; ↔ no clear change; ✓ FDR-significant vs injury; • trend (q≈0.05–0.10); n.t. not tested; Grey-shaded cells indicate conditions not tested in GMH. Cosine score reflects similarity of treated microglial transcriptome to healthy controls (higher is better)

This scoring system is a valuable template for screening treatment paradigms across neurological disorders, as screening can be undertaken more quickly than previous approaches.

This paper introduces a computational scoring s ystem that has substantial positive attributes for studying neuroprotective agents. While several prior animal scoring systems exist, such as Ozaydin et al. [62] who developed a hippocampal gross-pathology score (0–6) for neonatal HI in mice, Yang and Kuan [63] who used morphological assessments quantify white matter and BBB injury via histology in the HI model, and a model to link cell death with a categorical injury score in a piglet model of HI [64]. These approaches tend to focus on structural damage in single models and use categorical or semi-quantitative metrics. In contrast, our approach combines core histological markers (MBP/MAP2) with CNS-system-level immune balance indices (MG-transcriptomics). This means that the scoring system provides input into the functional tissue-level outcomes and the trajectory of (immune-mediated) changes occurring. This makes our scoring system agnostic to the therapeutic agent, as it is based on the response of microglia, which play a central role in almost every neurological and neurodegenerative disorder studied [65–68], as well as core structural protein indices that would be valuable to improve across therapies. In addition, prior approaches for compressing complex data have relied on categorical scales (mild/moderate/severe) [69, 70], but the cosine score allows for data compression with a continuous, quantitative metric, allowing sensitivity to subtle treatment effects.

A key limitation in the field of MSC research is the low standardisation of the process for their isolation, characterisation and expansion. The HuMSCs used in these experiments are research-grade, manufactured by a leader in the field (Lonza), and their quality was controlled through strict and specific analytical testing prior to use. The HuMSC were derived from the stromal Wharton's Jelly of the umbilical cord, characterised by APCDD1 expression and lack of 3G5 expression. This contrasts with HuMSCs derived from the perivascular area of the umbilical cord that express 3G5 and lack APCDD1 expression. The stromal Wharton's Jelly was chosen as the source instead of the perivascular area to ensure a uniform HuMSC cell population due to the contiguity of the perivascular area to the umbilical blood vessels. The umbilical cord was preferred over bone marrow because HuMSC can be obtained through ex vivo methodology. We decided on the doses in this study based on previous work from members of the PREMSTEM

consortium (www.premstem.eu) [40, 71–73] and the work of others in this area [74].

Treatment with HuMSC was most effective in both models when they were administered in the tertiary phase [75, 76], at least 15 days after the injury, which in the rat is equivalent to 2–3 years of age in a child [77]. In contrast, the P5 treatment is arguably equivalent to mid-to-late-term, and the P10 is equivalent to term age. This observation is therapy-specific, and we do not advocate withholding proven acute phase neuro-repair interventions as they become available. Instead, our pipeline supports a stratified strategy: apply early care universally, then offer HuMSC to those with confirmed deficits or persistent risk (discussed further below). The effectiveness of HuMSC treatment in the tertiary phase is supported by an increasing body of clinical evidence, which suggests that there are persisting facets of injury that may be targeted for intervention. These include biochemical data that changes in brain metabolites persist for at least one year after a hypoxic-ischemic (HI) injury at birth [78] and that there are neuroinflammatory changes after preterm birth that continue into childhood [79] and young adulthood [80]. In addition, there is evidence that peripheral immune cells are primed to respond more vigorously in children born preterm [81].

Preclinical evidence demonstrates that processes in the tertiary phase after perinatal brain injury are viable neurotherapeutic targets. For example, in models of term infant HI encephalopathy, improved outcomes have been reported when lithium treatment was initiated five days post-injury [82] and when methylprednisolone treatment was initiated seven days after injury [83]. Stem cells are also effective when administered in the tertiary phase in models of term infant HI encephalopathy. Specifically, adult adipose-derived MSCs reduced lesion size when administered with a delay of seven days post-injury [84], and bone marrow-derived MSCs reduced lesion size when delivered three days post-injury in a model of neonatal stroke [85], and in a model of HI encephalopathy [86]. In the second HI study by van Velthoven and colleagues, MSC treatment remained partially effective in this severe injury model, even when administered with a 10-day delay. Extensive cell death is a characteristic of these HI models and our GMH model. However, in the inflammation-induced EoP model, cell death does not play a significant role in injury [44], which is consistent with observations in human infants with moderate white matter injury [17, 87]. However, previous work also supports our observation that tertiary-phase MSC treatments are effective in inflammation-mediated injury models, characterised by low cell death. Specifically, in a model of maternal immune activation (MIA, E14.5 polyriboinosinic-polyribocytidylic acid, Poly I:C, exposure) changes in the adult offspring linked to persisting microglia dysfunction could be overcome with the application in the tertiary phase via deep brain stimulation [88] or modulation of the brain-derived neurotrophic factor (BDNF) pathway [89].

We found that MSC treatment trended to reduce the amount of myelin (i.e., caused more injury) in the inflammation-associated model of EoP when 20 M cells/kg were administered at P5. Reports on the efficacy of stem cells in preclinical models are overall very positive, although there are examples where they have been shown to have no effect or do further damage [90, 91], and the field of stem cell regeneration struggles with publication bias [92–94]. Acute-phase treatment with MSCs might have led to poorer outcomes than tertiary treatments due to the impact of the tissue milieu on the MSCs. Specifically, studies primarily in adults have shown that the early classically pro-inflammatory environment in the injured brain negatively affects the overall regenerative abilities of stem cells, as reviewed in [95]. Counter-intuitively, pre-conditioning MSC before delivery with stimuli that may be considered 'negative', such as hypoxia or pro-inflammatory cytokines, improves the abilities of MSC to repair the brain when delivered in vivo, as reviewed in [96]. However, the in vitro pre-conditioning exposes cells to simple and arguably mild stimuli compared with an in vivo injury setting. This leads us to hypothesise that striking differences between the in vitro and in vivo milieu easily explain why in vitro pre-conditioning can lead to better outcomes, but MSCs conditioned by delivery into the acute phase brain failed to be protective.

It is established that microglia play critical roles in causing perinatal brain injury [14, 19, 97] and undertake vital roles in all stages of brain development and adult brain health, reviewed in [98, 99]. Underpinning these strikingly different functions over time are distinct transcriptional profiles across development [20, 100]. In this study, we verified a temporal profile of response to inflammation-induced injury to model EoP in rats, which we have well-characterised in mice [19, 57, 101]. MSCs are competent in reducing the classically pro-inflammatory activation states of microglia [102, 103]. However, another avenue for future research is to study whether MSC treatment may improve outcomes by 'reactivating' microglia to a developmentally permissive state, wherein they are transcriptionally primed to stimulate myelination [15, 104, 105].

Treatments with strong potential for efficacy that can be delivered in the tertiary phase significantly benefit clinical trial design for infants with EoP. A substantial problem with undertaking clinical trials of acute phase treatments is that approximately 50% of preterm infants will do well on two-year outcome tests irrespective of any treatment, and we cannot effectively predict which infants will do well even with early clinical imaging.

There are even significant limitations in the abilities of the current 'gold standard' behavioural assessments (such as Bayley's III) at two years of age to predict longer-term outcomes, especially in very preterm born infants [106, 107]. Thus, if you treat all preterm-born infants in the acute phase when you observe them at follow-up, it is impossible to discriminate between those who would have done well, irrespective of treatment and those who responded positively to the therapy. This statistical dilemma has implications for trial size (increasing time and cost) and leads us to deliver therapies to babies who do not need them. Although we strongly advocate for the development and application of treatments for the acute phase if they can be effective, our data suggest that it may not be 'too late' to treat brain injury once it can be reliably established that changes to the developmental trajectory have occurred. As such, our data suggests that while there are no effective acute phase therapies for brain injury, a viable strategy could be to deliver HuMSC therapies to infants only once neurological issues are diagnosed. Significant advances in gross motor analyses make it possible for children to be reliably detected as high risk at 6–12 months in the case of cerebral palsy [108] or at 3–5 years in the case of neurodevelopmental disorders such as autism spectrum disorders or attention deficit hyperactivity disorder [109]. Our data suggests that stem cells could be ideal therapeutics for tertiary-phase treatments, allowing treatment to be delivered only once any impact of perinatal brain injury is proven, and perhaps as an adjunct to acute phase therapies as they become available.

Our project goal was to establish a simple, reproducible scoring system based on core histological and transcriptomic readouts. Moving towards clinical application, validating efficacy with additional physiological or biomarker datasets is essential. For example, future use should incorporate bedside tools such as near-infrared spectroscopy (NIRS) or cerebral Doppler, along with cerebrospinal fluid (CSF) or plasma cytokine profiling, which could provide complementary information to be evaluated in large animal models as part of the translational process [110–112]. These methods might ultimately help refine patient selection and optimal timing for treatment, and it will be crucial to study how these clinical indices align with the scoring system we outline.

In conclusion, this study highlights how a combination of computational biology and gold-standard neuropathology can allow researchers to test the effectiveness of many treatment permutations for perinatal brain injury faster and more efficiently. Now that we have established the pipeline for this approach, this type of screening could improve the cost- and time-effectiveness of testing therapies for many disorders.

Supplementary Information

The online version contains supplementary material available at https://doi.org/10.1186/s12974-025-03593-2.

Supplementary material 1

Supplementary material 2

Acknowledgements
Figure 1 was created with BioRender (Biorender.com).

Authors' contributions
Study concept and design: CB, CR, SN, CN, CDT, BF, JVS, ADD, HH, PG. Data acquisition and analysis: CB, CR, SN, DG, ERF, VF, TLC, CN, CDT., SLebon, JE, MGH, LS, MB, Kd, SLemoine, BF, JVS, ADD, HH, PG. Data interpretation and manuscript drafting: CB, CR, SN, DG, ERF, VF, TLC, CN, CDT, SB, LS, MB, KD, GV, NP, SL, BF, JVS, ADD, HH, PG.

Funding
This study was supported by grants from Inserm, Université Paris Cité, Horizon 2020 Framework Program of the European Union (grant agreement no. 874721/PREMSTEM), ERANET-NEURON (TRAINS), France 2030, Fondation de France, Fondation pour la Recherche Médicale, Fondation Grace de Monaco, Fondation des Gueules Cassées, Fondation Roger de Spoelberch, the national infrastructure of France Génomique, and additional grants from "Investissement d'Avenir -ANR-11-INBS-0011-" NeurATRIS and from "Investissement d'Avenir -ANR-10-INBS-09-". The authors acknowledge financial support from the Department of Health via the National Institute for Health Research (NIHR) comprehensive Biomedical Research Centre award to Guy's & St Thomas' NHS Foundation Trust in partnership with King's College London and King's College Hospital NHS Foundation Trust. The authors acknowledge financial support from a Ph.D. fellowship from Université Paris Cité (Ecole Doctorale BioSPC to CB), the EUR GENE (reference #ANR-17-EURE-0013) and is part of the Université Paris Cité IdEx #ANR-18-IDEX-0001 funded by the French Government through its "Investments for the Future" program. The authors acknowledge financial support from the "Digital health challenge" Inserm-CNRS joint program, the French Ministry of Higher Education and Research (reference #ENS.X19RDTME-SACLAY19-22), and the French National Research Agency (references ANR-19-CE23-0026–04, ANR-18-CE17-0009–01, ANR-21-RHUS-009, ANR-23-IAHU-0010). The study was supported by grants from the Swedish state under the agreement between the Swedish government and the county councils, the ALF agreement (ALFGBG-965174) and the Swedish Research Council (VR; 2019–01320; 2023–02035).
The supporting bodies played no role in any aspect of the study design, analysis, interpretation, or decision to publish this data.

Data availability
The datasets analysed during the current study are available in the GSE298271, and the datasets generated during the current study are available in the GitHub repository, https://github.com/INSERM-U1141-Neurodiderot/premstem-scoring.

Declarations

Ethics approval and consent to participate
Not applicable.

Consent for publication
Not applicable.

Competing interests
This research was conducted within the funding framework of PREMSTEM, a Horizons 2020 funded consortium (grant agreement no. 874721/PREMSTEM) The HuMSC used in this study were provided by Chiesi Farmaceutici, one of the members of the consortium. Chiesi Farmaceutici played no part in the design, execution and analysis of the data and did not play a role in the decision to publish or the data to be published. Their permission to publish has been obtained.

Author details
[1]Université Paris Cité, NeuroDiderot, Inserm, Paris 75019, France
[2]Centre of Perinatal Medicine and Health, Sahlgrenska Academy, University of Gothenburg, Gothenburg, Sweden
[3]Institute of Clinical Sciences and Neuroscience and Physiology, Sahlgrenska Academy, University of Gothenburg, Gothenburg, Sweden
[4]Department of Pharmacy, AP-HP, Robert Debré Hospital, Paris 75019, France
[5]Department for Developmental Origins of Disease, University Medical Center Utrecht, Utrecht University, Utrecht, The Netherlands
[6]Département de Biologie, Genomique ENS, Institut de Biologie de L'ENS (IBENS), École Normale Supérieure, CNRS, INSERM, Université PSL, Paris 75005, France
[7]Global Rare Diseases, Chiesi Farmaceutici S.P.A., Parma 43122, Italy
[8]Global R&D, Chiesi Farmaceutici S.P.A., Parma 43122, Italy
[9]School of Health and Biomedical Sciences, STEM College, RMIT University, Bundoora, VIC 3083, Australia
[10]Université Sorbonne Paris Nord, UFR de Santé, Médecine Et Biologie Humaine, Bobigny 93000, France
[11]Unité Fonctionnelle de Médecine Génomique Et Génétique Clinique, Hôpital Jean Verdier, AP-HP, Bondy 93140, France

Received: 16 July 2025 / Accepted: 8 October 2025
Published online: 23 December 2025

References

1. Simoens S, Huys I. R&D costs of new medicines: a landscape analysis. Front Med. 2021;8:760762. https://doi.org/10.3389/fmed.2021.760762.
2. Lu Q, An WF. Impact of novel screening technologies on ion channel drug discovery. Comb Chem High Throughput Screen. 2008;11:185–94. https://doi.org/10.2174/138620708783877735.
3. Nero TL, Morton CJ, Holien JK, Wielens J, Parker MW. Oncogenic protein interfaces: small molecules, big challenges. Nat Rev Cancer. 2014;14:248–62. https://doi.org/10.1038/nrc3690.
4. Hee Chung E, Chou J, Brown KA. Neurodevelopmental outcomes of preterm infants: a recent literature review. Transl Pediatr. 2020;9:S3–8. https://doi.org/10.21037/tp.2019.09.10.
5. D'Onofrio BM, Class QA, Rickert ME, Larsson H, Langstrom N, Lichtenstein P. Preterm birth and mortality and morbidity: a population-based quasi-experimental study. JAMA Psychiatry. 2013;70:1231–40. https://doi.org/10.1001/jamapsychiatry.2013.2107.
6. Crump C, Sundquist J, Sundquist K. Stroke risks in adult survivors of preterm birth: national cohort and cosibling study. Stroke. 2021;52:2609–17. https://doi.org/10.1161/STROKEAHA.120.033797.
7. Heinonen K, Eriksson JG, Lahti J, Kajantie E, Pesonen AK, Tuovinen S, et al. Late preterm birth and neurocognitive performance in late adulthood: a birth cohort study. Pediatrics. 2015;135:e818-825. https://doi.org/10.1542/peds.2014-3556.
8. Azzopardi D, Robertson NJ, Bainbridge A, Cady E, Charles-Edwards G, Deierl A, et al. Moderate hypothermia within 6 h of birth plus inhaled xenon versus moderate hypothermia alone after birth asphyxia (TOBY-Xe): a proof-of-concept, open-label, randomised controlled trial. Lancet Neurol. 2016;15:145–53. https://doi.org/10.1016/S1474-4422(15)00347-6.
9. Porter EJ, Counsell SJ, Edwards AD, Allsop J, Azzopardi D. Tract-based spatial statistics of magnetic resonance images to assess disease and treatment effects in perinatal asphyxial encephalopathy. Pediatr Res. 2010;68:205–9. https://doi.org/10.1203/PDR.0b013e3181e9f1ba.
10. Du X, Fleiss B, Li H, D'Angelo B, Sun Y, Zhu C, et al. Systemic stimulation of TLR2 impairs neonatal mouse brain development. PLoS One. 2011;6:e19583. https://doi.org/10.1371/journal.pone.0019583.
11. Gussenhoven R, Westerlaken RJJ, Ophelders D, Jobe AH, Kemp MW, Kallapur SG, et al. Chorioamnionitis, neuroinflammation, and injury: timing is key in the preterm ovine fetus. J Neuroinflammation. 2018;15:113. https://doi.org/10.1186/s12974-018-1149-x.
12. Hagberg H, Mallard C, Ferriero DM, Vannucci SJ, Levison SW, Vexler ZS, et al. The role of inflammation in perinatal brain injury. Nat Rev Neurol. 2015;11:192–208. https://doi.org/10.1038/nrneurol.2015.13.
13. Haynes RL, van Leyen K. 12/15-lipoxygenase expression is increased in oligodendrocytes and microglia of periventricular leukomalacia. Dev Neurosci. 2013;35:140–54. https://doi.org/10.1159/000350230.
14. Holloway RK, Ireland G, Sullivan G, Becher JC, Smith C, Boardman JP, et al. Microglial inflammasome activation drives developmental white matter injury. Glia. 2021;69:1268–80. https://doi.org/10.1002/glia.23963.
15. Holloway RK, Zhang L, Molina-Gonzalez I, Ton K, Nicoll JAR, Boardman JP, et al. Localized microglia dysregulation impairs central nervous system myelination in development. Acta Neuropathol Commun. 2023;11:49. https://doi.org/10.1186/s40478-023-01543-8.
16. Schmidt AF, Kannan PS, Chougnet CA, Danzer SC, Miller LA, Jobe AH, et al. Intra-amniotic LPS causes acute neuroinflammation in preterm rhesus macaques. J Neuroinflammation. 2016;13:238. https://doi.org/10.1186/s12974-016-0706-4.
17. Verney C, Pogledic I, Biran V, Adle-Biassette H, Fallet-Bianco C, Gressens P. Microglial reaction in axonal crossroads is a hallmark of noncystic periventricular white matter injury in very preterm infants. J Neuropathol Exp Neurol. 2012;71:251–64. https://doi.org/10.1097/NEN.0b013e3182496429.
18. Dean JM, Wang X, Kaindl AM, Gressens P, Fleiss B, Hagberg H, et al. Microglial MyD88 signaling regulates acute neuronal toxicity of LPS-stimulated microglia in vitro. Brain Behav Immun. 2010;24:776–83. https://doi.org/10.1016/j.bbi.2009.10.018.
19. Van Steenwinckel J, Schang AL, Krishnan ML, Degos V, Delahaye-Duriez A, Bokobza C, et al. Decreased microglial Wnt/β-catenin signalling drives microglial pro-inflammatory activation in the developing brain. Brain. 2019;142:3806–33. https://doi.org/10.1093/brain/awz319.
20. Matcovitch-Natan O, Winter DR, Giladi A, Vargas Aguilar S, Spinrad A, Sarrazin S, et al. Microglia development follows a stepwise program to regulate brain homeostasis. Science. 2016;353:aad8670. https://doi.org/10.1126/science.aad8670.
21. Paolicelli RC, Bolasco G, Pagani F, Maggi L, Scianni M, Panzanelli P, et al. Synaptic pruning by microglia is necessary for normal brain development. Science. 2011;333:1456–8. https://doi.org/10.1126/science.1202529.
22. Zhan Y, Paolicelli RC, Sforazzini F, Weinhard L, Bolasco G, Pagani F, et al. Deficient neuron-microglia signaling results in impaired functional brain connectivity and social behavior. Nat Neurosci. 2014;17:400–6. https://doi.org/10.1038/nn.3641.
23. Cappelletti M, Doll JR, Stankiewicz TE, Lawson MJ, Sauer V, Wen B, et al. Maternal regulation of inflammatory cues is required for induction of preterm birth. JCI Insight. 2020. https://doi.org/10.1172/jci.insight.138812.
24. Romero R, Velez Edwards DR, Kusanovic JP, Hassan SS, Mazaki-Tovi S, Vaisbuch E, et al. Identification of fetal and maternal single nucleotide polymorphisms in candidate genes that predispose to spontaneous preterm labor with intact membranes. Am J Obstet Gynecol. 2010;202(431):e431-434. https://doi.org/10.1016/j.ajog.2010.03.026.
25. Cai S, Thompson DK, Anderson PJ, Yang JY. Short- and long-term neurodevelopmental outcomes of very preterm infants with neonatal sepsis: a systematic review and meta-analysis. Children (Basel). 2019. https://doi.org/10.3390/children6120131.
26. Leviton A, Allred EN, Fichorova RN, Kuban KC, Michael O'Shea T, Dammann O. Systemic inflammation on postnatal days 21 and 28 and indicators of brain dysfunction 2 years later among children born before the 28th week of gestation. Early Hum Dev. 2016;93:25–32. https://doi.org/10.1016/j.earlhumdev.2015.11.004.
27. O'Shea TM, Allred EN, Kuban KC, Dammann O, Paneth N, Fichorova R, et al. Elevated concentrations of inflammation-related proteins in postnatal blood predict severe developmental delay at 2 years of age in extremely preterm infants. J Pediatr. 2012;160:395-401 e394. https://doi.org/10.1016/j.jpeds.2011.08.069.
28. Tsamantioti E, Lisonkova S, Muraca G, Ortqvist AK, Razaz N. Chorioamnionitis and risk of long-term neurodevelopmental disorders in offspring: a population-based cohort study. Am J Obstet Gynecol. 2022;227:287 e281-287 e217. https://doi.org/10.1016/j.ajog.2022.03.028.
29. Klein L, Van Steenwinckel J, Fleiss B, Scheuer T, Buhrer C, Faivre V, et al. A unique cerebellar pattern of microglia activation in a mouse model of encephalopathy of prematurity. Glia. 2022;70:1699–719. https://doi.org/10.1002/glia.24190.
30. Schang AL, Van Steenwinckel J, Ioannidou ZS, Lipecki J, Rich-Griffin C, Woolley-Allen K, et al. Epigenetic priming of immune/inflammatory pathways activation and abnormal activity of cell cycle pathway in a perinatal model of white matter injury. Cell Death Dis. 2022;13:1038. https://doi.org/10.1038/s41419-022-05483-4.
31. Veerasammy S, Van Steenwinckel J, Le Charpentier T, Seo JH, Fleiss B, Gressens P, et al. Perinatal IL-1beta-induced inflammation suppresses Tbr2(+) intermediate progenitor cell proliferation in the developing hippocampus

accompanied by long-term behavioral deficits. Brain Behav Immun Health. 2020;7:100106. https://doi.org/10.1016/j.bbih.2020.100106.
32. Yates AG, Kislitsyna E, Alfonso Martin C, Zhang J, Sewell AL, Goikolea-Vives A, et al. Montelukast reduces grey matter abnormalities and functional deficits in a mouse model of inflammation-induced encephalopathy of prematurity. J Neuroinflammation. 2022;19:265. https://doi.org/10.1186/s12974-022-02625-5.
33. Hefti MM, Trachtenberg FL, Haynes RL, Hassett C, Volpe JJ, Kinney HC. A century of germinal matrix intraventricular hemorrhage in autopsied premature infants: a historical account. Pediatr Dev Pathol. 2016;19:108–14. https://doi.org/10.2350/15-06-1663-OA.1.
34. Jinnai M, Koning G, Singh-Mallah G, Jonsdotter A, Leverin A-L, Svedin P, et al. A model of germinal matrix hemorrhage in preterm rat pups. Front Cell Neurosci. 2020. https://doi.org/10.3389/fncel.2020.535320.
35. Song J, Nilsson G, Xu Y, Zelco A, Rocha-Ferreira E, Wang Y, et al. Temporal brain transcriptome analysis reveals key pathological events after germinal matrix hemorrhage in neonatal rats. J Cereb Blood Flow Metab. 2022;42:1632–49. https://doi.org/10.1177/0271678X221098811.
36. Jellema RK, Wolfs TG, Lima Passos V, Zwanenburg A, Ophelders DR, Kuypers E, et al. Mesenchymal stem cells induce T-cell tolerance and protect the preterm brain after global hypoxia-ischemia. PloS One. 2013;8:e73031. https://doi.org/10.1371/journal.pone.0073031.
37. Li J, Yawno T, Sutherland AE, Gurung S, Paton M, McDonald C, et al. Preterm umbilical cord blood derived mesenchymal stem/stromal cells protect preterm white matter brain development against hypoxia-ischemia. Exp Neurol. 2018;308:120–31. https://doi.org/10.1016/j.expneurol.2018.07.006.
38. Malhotra A, Thebaud B, Paton MCB, Fleiss B, Papagianis P, Baker E, et al. Advances in neonatal cell therapies: proceedings of the first neonatal cell therapies symposium (2022). Pediatr Res. 2023;94:1631–8. https://doi.org/10.1038/s41390-023-02707-x.
39. Nair S, Rocha-Ferreira E, Fleiss B, Nijboer CH, Gressens P, Mallard C, et al. Neuroprotection offered by mesenchymal stem cells in perinatal brain injury: role of mitochondria, inflammation, and reactive oxygen species. J Neurochem. 2021;158:59–73. https://doi.org/10.1111/jnc.15267.
40. Vaes JEG, van Kammen CM, Trayford C, van der Toorn A, Ruhwedel T, Benders M, et al. Intranasal mesenchymal stem cell therapy to boost myelination after encephalopathy of prematurity. Glia. 2021;69:655–80. https://doi.org/10.1002/glia.23919.
41. Passera S, Boccazzi M, Bokobza C, Faivre V, Mosca F, Van Steenwinckel J, et al. Therapeutic potential of stem cells for preterm infant brain damage: can we move from the heterogeneity of preclinical and clinical studies to established therapeutics? Biochem Pharmacol. 2021;186:114461. https://doi.org/10.1016/j.bcp.2021.114461.
42. Razak A, Lei D, McDonald CA, Hunt RW, Miller SL, Malhotra A. Allogeneic cell therapy applications in neonates: a systematic review. Stem Cells Transl Med. 2023. https://doi.org/10.1093/stcltm/szad048.
43. Zhou L, McDonald C, Yawno T, Jenkin G, Miller S, Malhotra A. Umbilical cord blood and cord tissue-derived cell therapies for neonatal morbidities: current status and future challenges. Stem Cells Transl Med. 2022;11:135–45. https://doi.org/10.1093/stcltm/szab024.
44. Favrais G, van de Looij Y, Fleiss B, Ramanantsoa N, Bonnin P, Stoltenburg-Didinger G, et al. Systemic inflammation disrupts the developmental program of white matter. Ann Neurol. 2011;70:550–65. https://doi.org/10.1002/ana.22489.
45. Shiow LR, Favrais G, Schirmer L, Schang AL, Cipriani S, Andres C, et al. Reactive astrocyte COX2-PGE2 production inhibits oligodendrocyte maturation in neonatal white matter injury. Glia. 2017;65:2024–37. https://doi.org/10.1002/glia.23212.
46. Stolp HB, Fleiss B, Arai Y, Supramaniam V, Vontell R, Birtles S, et al. Interneuron development is disrupted in preterm brains with diffuse white matter injury: observations in mouse and human. Front Physiol. 2019;10:955. https://doi.org/10.3389/fphys.2019.00955.
47. Andersson EA, Rocha-Ferreira E, Hagberg H, Mallard C, Ek CJ. Function and biomarkers of the blood-brain barrier in a neonatal germinal matrix haemorrhage model. Cells. 2021. https://doi.org/10.3390/cells10071677.
48. Percie du Sert N, Hurst V, Ahluwalia A, Alam S, Avey MT, Baker M, et al. The ARRIVE guidelines 2.0: updated guidelines for reporting animal research. BMJ Open Sci. 2020;4:e100115. https://doi.org/10.1136/bmjos-2020-100115.
49. Mairesse J, Zinni M, Pansiot J, Hassan-Abdi R, Demene C, Colella M, et al. Oxytocin receptor agonist reduces perinatal brain damage by targeting microglia. Glia. 2019;67:345–59. https://doi.org/10.1002/glia.23546.
50. Kelly LA, Branagan A, Semova G, Molloy EJ. Sex differences in neonatal brain injury and inflammation. Front Immunol. 2023;14:1243364. https://doi.org/10.3389/fimmu.2023.1243364.
51. Jourdren L, Bernard M, Dillies MA, Le Crom S. Eoulsan: a cloud computing-based framework facilitating high throughput sequencing analyses. Bioinformatics. 2012;28:1542–3. https://doi.org/10.1093/bioinformatics/bts165.
52. Dobin A, Davis CA, Schlesinger F, Drenkow J, Zaleski C, Jha S, et al. STAR: ultrafast universal RNA-seq aligner. Bioinformatics. 2013;29:15–21. https://doi.org/10.1093/bioinformatics/bts635.
53. Li H, Handsaker B, Wysoker A, Fennell T, Ruan J, Homer N, et al. The sequence alignment/map format and SAMtools. Bioinformatics. 2009;25:2078–9. https://doi.org/10.1093/bioinformatics/btp352.
54. Anders S, Pyl PT, Huber W. HTSeq–a python framework to work with high-throughput sequencing data. Bioinformatics. 2015;31:166–9. https://doi.org/10.1093/bioinformatics/btu638.
55. Love MI, Huber W, Anders S. Moderated estimation of fold change and dispersion for RNA-seq data with DESeq2. Genome Biol. 2014;15:550. https://doi.org/10.1186/s13059-014-0550-8.
56. Clark NR, Hu KS, Feldmann AS, Kou Y, Chen EY, Duan Q, et al. The characteristic direction: a geometrical approach to identify differentially expressed genes. BMC Bioinform. 2014;15:79. https://doi.org/10.1186/1471-2105-15-79.
57. Krishnan ML, Van Steenwinckel J, Schang AL, Yan J, Arnadottir J, Le Charpentier T, et al. Integrative genomics of microglia implicates DLG4 (PSD95) in the white matter development of preterm infants. Nat Commun. 2017;8:428. https://doi.org/10.1038/s41467-017-00422-w.
58. Bokobza C, Jacquens A, Zinni M, Faivre V, Hua J, Guenoun D, Userovici C, Mani S, Degos V, Gressens P, Van Steenwinckel J. Magnetic isolation of microglial cells from neonate mouse for primary cell cultures. J Vis Exp. 2022. https://doi.org/10.3791/62964.
59. Bokobza C, Joshi P, Schang AL, Csaba Z, Faivre V, Montane A, et al. miR-146b protects the perinatal brain against microglia-induced hypomyelination. Ann Neurol. 2022;91:48–65. https://doi.org/10.1002/ana.2626.
60. Boccazzi M, Van Steenwinckel J, Schang AL, Faivre V, Le Charpentier T, Bokobza C, et al. The immune-inflammatory response of oligodendrocytes in a murine model of preterm white matter injury: the role of TLR3 activation. Cell Death Dis. 2021;12:166. https://doi.org/10.1038/s41419-021-03446-9.
61. Rangon CM, Schang AL, Van Steenwinckel J, Schwendimann L, Lebon S, Fu T, et al. Myelination induction by a histamine H3 receptor antagonist in a mouse model of preterm white matter injury. Brain Behav Immun. 2018. https://doi.org/10.1016/j.bbi.2018.09.017.
62. Ozaydin B, Bicki E, Taparli OE, Sheikh TZ, Schmidt DK, Yapici S, et al. Novel injury scoring tool for assessing brain injury following neonatal hypoxia-ischemia in mice. Dev Neurosci. 2022;44:394–411. https://doi.org/10.1159/000525244.
63. Yang D, Kuan C-Y. Morphological assessments of neonatal hypoxia–ischemia: white matter and blood-brain barrier injury. In: Chen J, Xu X-M, Xu ZC, Zhang JH, editors. Animal models of acute neurological injuries II: injury and mechanistic assessments, vol. 2. Totowa, NJ: Humana Press; 2012. p. 201–10.
64. Hoque N, Sabir H, Maes E, Bishop S, Thoresen M. Validation of a neuropathology score using quantitative methods to evaluate brain injury in a pig model of hypoxia ischaemia. J Neurosci Methods. 2014;230:30–6. https://doi.org/10.1016/j.jneumeth.2014.04.005.
65. Fleiss B, Gressens P. Role of microglial modulation in therapies for perinatal brain injuries leading to neurodevelopmental disorders. Adv Neurobiol. 2024;37:591–606. https://doi.org/10.1007/978-3-031-55529-9_33.
66. Gagliano A, Cucinotta F, Giunta I, Di Modica I, De Domenico C, Costanza C, et al. The immune/inflammatory underpinnings of neurodevelopmental disorders and pediatric acute-onset neuropsychiatric syndrome: a scoping review. Int J Mol Sci. 2025. https://doi.org/10.3390/ijms26167767.
67. Gao C, Jiang J, Tan Y, Chen S. Microglia in neurodegenerative diseases: mechanism and potential therapeutic targets. Signal Transduct Target Ther. 2023;8:359. https://doi.org/10.1038/s41392-023-01588-0.
68. Zhu H, Guan A, Liu J, Peng L, Zhang Z, Wang S. Noteworthy perspectives on microglia in neuropsychiatric disorders. J Neuroinflammation. 2023;20:223. https://doi.org/10.1186/s12974-023-02901-y.
69. Nguyen LH, Holmes S. Ten quick tips for effective dimensionality reduction. PLoS Comput Biol. 2019;15:e1006907. https://doi.org/10.1371/journal.pcbi.1006907.
70. Schafer KA, Eighmy J, Fikes JD, Halpern WG, Hukkanen RR, Long GG, et al. Use of severity grades to characterize histopathologic changes. Toxicol Pathol. 2018;46:256–65. https://doi.org/10.1177/0192623318761348.

71. Corcelli M, Hawkins K, Vlahova F, Hunjan A, Dowding K, De Coppi P, et al. Neuroprotection of the hypoxic-ischemic mouse brain by human CD117(+) CD90(+)CD105(+) amniotic fluid stem cells. Sci Rep. 2018;8:2425. https://doi.org/10.1038/s41598-018-20710-9.
72. Herz J, Koster C, Reinboth BS, Dzietko M, Hansen W, Sabir H, et al. Interaction between hypothermia and delayed mesenchymal stem cell therapy in neonatal hypoxic-ischemic brain injury. Brain Behav Immun. 2018;70:118–30. https://doi.org/10.1016/j.bbi.2018.02.006.
73. Jellema RK, Ophelders DR, Zwanenburg A, Nikiforou M, Delhaas T, Andriessen P, et al. Multipotent adult progenitor cells for hypoxic-ischemic injury in the preterm brain. J Neuroinflammation. 2015;12:241. https://doi.org/10.1186/s12974-015-0459-5.
74. Davidson JO, van den Heuij LG, Fraser M, Wassink G, Miller SL, Lim R, et al. Window of opportunity for human amnion epithelial stem cells to attenuate astrogliosis after umbilical cord occlusion in preterm fetal sheep. Stem Cells Transl Med. 2021;10:427–40. https://doi.org/10.1002/sctm.20-0314.
75. Fleiss B, Gressens P. Tertiary mechanisms of brain damage: a new hope for treatment of cerebral palsy? Lancet Neurol. 2012;11:556–66. https://doi.org/10.1016/S1474-4422(12)70058-3.
76. Levison SW, Rocha-Ferreira E, Kim BH, Hagberg H, Fleiss B, Gressens P, Dobrowolski R. Mechanisms of tertiary neurodegeneration after neonatal hypoxic-ischemic brain damage. Pediatr Med. 2021. https://pm.amegroups.com/article/view/6124.
77. Semple BD, Blomgren K, Gimlin K, Ferriero DM, Noble-Haeusslein LJ. Brain development in rodents and humans: identifying benchmarks of maturation and vulnerability to injury across species. Prog Neurobiol. 2013;106:1–16. https://doi.org/10.1016/j.pneurobio.2013.04.001.
78. Robertson NJ, Cox IJ, Cowan FM, Counsell SJ, Azzopardi D, Edwards AD. Cerebral intracellular lactic alkalosis persisting months after neonatal encephalopathy measured by magnetic resonance spectroscopy. Pediatr Res. 1999;46:287–96. https://doi.org/10.1203/00006450-199909000-00007.
79. Van der Zwart S, Knol EF, Gressens P, Koopman C, Benders M, Roze E. Neuroinflammatory markers at school age in preterm born children with neurodevelopmental impairments. Brain Behav Immun. 2024;38:100791. https://doi.org/10.1016/j.bbih.2024.100791.
80. Cheong JL, Bainbridge A, Anderson PJ, Lee KJ, Burnett AC, Thompson DK, et al. Altered posterior cingulate brain metabolites and cognitive dysfunction in preterm adolescents. Pediatr Res. 2016;79:716–22. https://doi.org/10.1038/pr.2015.272.
81. Lin CY, Chang YC, Wang ST, Lee TY, Lin CF, Huang CC. Altered inflammatory responses in preterm children with cerebral palsy. Ann Neurol. 2010;68:204–12. https://doi.org/10.1002/ana.22049.
82. Xie C, Zhou K, Wang X, Blomgren K, Zhu C. Therapeutic benefits of delayed lithium administration in the neonatal rat after cerebral hypoxia-ischemia. PLoS One. 2014;9:e107192. https://doi.org/10.1371/journal.pone.0107192.
83. Altamentova S, Rumajogee P, Hong J, Beldick SR, Park SJ, Yee A, et al. Methylprednisolone reduces persistent post-ischemic inflammation in a rat hypoxia-ischemia model of perinatal stroke. Transl Stroke Res. 2020;11:1117–36. https://doi.org/10.1007/s12975-020-00792-2.
84. Basham HK, Aghoghovwia BE, Papaioannou P, Seo S, Oorschot DE. Delayed double treatment with adult-sourced adipose-derived mesenchymal stem cells increases striatal medium-spiny neuronal number, decreases striatal microglial number, and has no subventricular proliferative effect, after acute neonatal hypoxia-ischemia in male rats. Int J Mol Sci. 2021;22:7862. https://doi.org/10.3390/ijms22157862.
85. van Velthoven CT, Sheldon RA, Kavelaars A, Derugin N, Vexler ZS, Willemen HL, et al. Mesenchymal stem cell transplantation attenuates brain injury after neonatal stroke. Stroke. 2013;44:1426–32. https://doi.org/10.1161/STROKEAHA.111.000326.
86. van Velthoven CT, Kavelaars A, van Bel F, Heijnen CJ. Mesenchymal stem cell treatment after neonatal hypoxic-ischemic brain injury improves behavioral outcome and induces neuronal and oligodendrocyte regeneration. Brain Behav Immun. 2010;24:387–93. https://doi.org/10.1016/j.bbi.2009.10.017.
87. Billiards SS, Haynes RL, Folkerth RD, Borenstein NS, Trachtenberg FL, Rowitch DH, et al. Myelin abnormalities without oligodendrocyte loss in periventricular leukomalacia. Brain Pathol. 2008;18:153–63. https://doi.org/10.1111/j.1750-3639.2007.00107.x.
88. Hadar R, Dong L, Del-Valle-Anton L, Guneykaya D, Voget M, Edemann-Callesen H, et al. Deep brain stimulation during early adolescence prevents microglial alterations in a model of maternal immune activation. Brain Behav Immun. 2017;63:71–80. https://doi.org/10.1016/j.bbi.2016.12.003.
89. Han M, Zhang JC, Yao W, Yang C, Ishima T, Ren Q, et al. Intake of 7,8-dihydroxyflavone during juvenile and adolescent stages prevents onset of psychosis in adult offspring after maternal immune activation. Sci Rep. 2016;6:36087. https://doi.org/10.1038/srep36087.
90. Turtzo LC, Budde MD, Dean DD, Gold EM, Lewis BK, Janes L, et al. Failure of intravenous or intracardiac delivery of mesenchymal stromal cells to improve outcomes after focal traumatic brain injury in the female rat. PLoS One. 2015;10:e0126551. https://doi.org/10.1371/journal.pone.0126551.
91. Dalous J, Pansiot J, Pham H, Chatel P, Nadaradja C, D'Agostino I, Vottier G, Schwendimann L, Vanneaux V, Charriaut-Marlangue C, Titomanlio L, Gressens P, Larghero J, Baud O. Use of human umbilical cord blood mononuclear cells to prevent perinatal brain injury: a preclinical study. Stem Cells Dev. 2012. https://doi.org/10.1089/scd.2012.0183.
92. Chen L, Zhang G, Khan AA, Guo X, Gu Y. Clinical efficacy and meta-analysis of stem cell therapies for patients with brain ischemia. Stem Cells Int. 2016;2016(1):6129579. https://doi.org/10.1155/2016/6129579.
93. Deinsberger J, Reisinger D, Weber B. Global trends in clinical trials involving pluripotent stem cells: a systematic multi-database analysis. NPJ Regen Med. 2020;5:15. https://doi.org/10.1038/s41536-020-00100-4.
94. Peng W, Sun J, Sheng C, Wang Z, Wang Y, Zhang C, et al. Systematic review and meta-analysis of efficacy of mesenchymal stem cells on locomotor recovery in animal models of traumatic brain injury. Stem Cell Res Ther. 2015;6:47. https://doi.org/10.1186/s13287-015-0034-0.
95. Mathieu P, Battista D, Depino A, Roca V, Graciarena M, Pitossi F. The more you have, the less you get: the functional role of inflammation on neuronal differentiation of endogenous and transplanted neural stem cells in the adult brain. J Neurochem. 2010;112:1368–85. https://doi.org/10.1111/j.1471-4159.2009.06548.x.
96. Moeinabadi-Bidgoli K, Babajani A, Yazdanpanah G, Farhadihosseinabadi B, Jamshidi E, Bahrami S, et al. Translational insights into stem cell preconditioning: from molecular mechanisms to preclinical applications. Biomed Pharmacother. 2021;142:112026. https://doi.org/10.1016/j.biopha.2021.112026.
97. Tahraoui SL, Marret S, Bodenant C, Leroux P, Dommergues MA, Evrard P, et al. Central role of microglia in neonatal excitotoxic lesions of the murine periventricular white matter. Brain Pathol. 2001;11:56–71. http://www.ncbi.nlm.nih.gov/pubmed/11145204.
98. Fleiss B, Van Steenwinckel J, Bokobza C, Shearer KI, Ross-Munro E, Gressens P. Microglia-mediated neurodegeneration in perinatal brain injuries. Biomolecules. 2021;11:99. https://doi.org/10.3390/biom11010099.
99. McNamara NB, Munro DAD, Bestard-Cuche N, Uyeda A, Bogie JFJ, Hoffmann A, et al. Microglia regulate central nervous system myelin growth and integrity. Nature. 2023;613:120–9. https://doi.org/10.1038/s41586-022-05534-y.
100. Hammond TR, Dufort C, Dissing-Olesen L, Giera S, Young A, Wysoker A, et al. Single-cell RNA sequencing of microglia throughout the mouse lifespan and in the injured brain reveals complex cell-state changes. Immunity. 2019;50:253-271 e256. https://doi.org/10.1016/j.immuni.2018.11.004.
101. Dufour A, Heydari Olya A, Foulon S, Reda C, Mokhtari A, Faivre V, et al. Neonatal inflammation impairs developmentally-associated microglia and promotes a highly reactive microglial subset. Brain Behav Immun. 2025;123:466–82. https://doi.org/10.1016/j.bbi.2024.09.019.
102. Liu Y, Zhang R, Yan K, Chen F, Huang W, Lv B, et al. Mesenchymal stem cells inhibit lipopolysaccharide-induced inflammatory responses of BV2 microglial cells through TSG-6. J Neuroinflammation. 2014;11:135. https://doi.org/10.1186/1742-2094-11-135.
103. Zanier ER, Pischiutta F, Riganti L, Marchesi F, Turola E, Fumagalli S, et al. Bone marrow mesenchymal stromal cells drive protective M2 microglia polarization after brain trauma. Neurotherapeutics. 2014;11:679–95. https://doi.org/10.1007/s13311-014-0277-y.
104. Lloyd AF, Miron VE. The pro-remyelination properties of microglia in the central nervous system. Nat Rev Neurol. 2019. https://doi.org/10.1038/s41582-019-0184-2.
105. Wlodarczyk A, Holtman IR, Krueger M, Yogev N, Bruttger J, Khorooshi R, et al. A novel microglial subset plays a key role in myelinogenesis in developing brain. EMBO J. 2017. https://doi.org/10.15252/embj.201696056.
106. Spittle AJ, Lee KJ, Spencer-Smith M, Lorefice LE, Anderson PJ, Doyle LW. Accuracy of two motor assessments during the first year of life in preterm infants for predicting motor outcome at preschool age. PLoS One. 2015;10:e0125854. https://doi.org/10.1371/journal.pone.0125854.
107. Spittle AJ, Spencer-Smith MM, Eeles AL, Lee KJ, Lorefice LE, Anderson PJ, et al. Does the Bayley-III motor scale at 2 years predict motor outcome at 4 years in very preterm children? Dev Med Child Neurol. 2013;55:448–52. https://doi.org/10.1111/dmcn.12049.

108. Malhotra A. Editorial: early detection and early intervention strategies for cerebral palsy in low and high resource settings. Brain Sci. 2022. https://doi.org/10.3390/brainsci12080960.
109. Solmi M, Radua J, Olivola M, Croce E, Soardo L, Salazar de Pablo G, et al. Age at onset of mental disorders worldwide: large-scale meta-analysis of 192 epidemiological studies. Mol Psychiatry. 2022;27:281–95. https://doi.org/10.1038/s41380-021-01161-7.
110. Inocencio IM, Kaur N, Tran NT, Wong FY. Cerebral haemodynamic response to somatosensory stimulation in preterm lambs is enhanced following sildenafil and inhaled nitric oxide administration. Front Physiol. 2023;14:1101647. https://doi.org/10.3389/fphys.2023.1101647.
111. Lingam I, Avdic-Belltheus A, Meehan C, Martinello K, Ragab S, Peebles D, et al. Serial blood cytokine and chemokine mRNA and microRNA over 48 h are insult specific in a piglet model of inflammation-sensitized hypoxia-ischaemia. Pediatr Res. 2021;89:464–75. https://doi.org/10.1038/s41390-020-0986-3.
112. Pang R, Meehan C, Maple G, Norris G, Campbell E, Tucker K, et al. Melatonin reduces brain injury following inflammation-amplified hypoxia-ischemia in a translational newborn piglet study of neonatal encephalopathy. J Pineal Res. 2024;76:e12962. https://doi.org/10.1111/jpi.12962.

Publisher's Note